

Re-Review of Yue et al., ACPD “Ozone and haze pollution weakens net primary productivity in China”

We are grateful to the reviewer for their time and energy in providing helpful comments and guidance that have improved the manuscript. In this document, we describe how we have addressed the reviewer’s comments. Referee comments are shown in black italics (first round) and light blue (second round). Author responses are shown in blue (first round) and magenta (second round) regular text.

I appreciate the authors’ efforts to address the review comments. I would like to see a little more information on some of the points raised and I include some additional minor points below.

3. The paper needs a more consistent time-scale. The overall results are presented as annual, however all the figures (except Fig 10) show summertime results only. The authors should either include evaluation for all seasons (or annual means), or present the final results only for summer. As is, the reader cannot judge model skill or response for other seasons.

→ The reason why our analyses and the Figures focus on the summer is that both GPP/NPP and air pollution (especially O₃) reach maximum at this season. The largest interactions between carbon flux and air pollution are found for this season. It is not a contradiction to show Figures on the summer average and provide annual average impacts because the carbon loss in summer largely dominates the annual total. We found that, for O₃ damages, “about 61% of such inhibition occurs in summer, when both photosynthesis and [O₃] reach maximum of the year.” (Lines 409-410). For the combined O₃ and aerosol effects, “a dominant fraction (60% without AIE and 52% with AIE) of the reduced carbon uptake occurs in summer, when both NPP and [O₃] reach maximum of the year.” (Lines 474-476). We also elect to present and summarize the annual average results to the reader for consistency with regional carbon budget studies. Having the annual average values easily available facilitates comparison with other carbon flux impacts and carbon emissions. For example, we found that: “the combined effects of O₃ and aerosols (Table 3) decrease total NPP in China by 0.39 (without AIE) to 0.80 Pg C yr⁻¹ (with AIE), equivalent to 9-16% of the pollution-free NPP and 16-32% of the total anthropogenic carbon emissions”. (Lines 469-471)

The authors themselves state that some of the results depend on the season (line 488) and this should be fully discussed. The authors may prefer to focus on summer in the main text Figures, but given that the impacts of other seasons are not negligible and the main conclusions are given as annual means, they MUST provide additional model evaluation in non-summer seasons in the Supplementary Materials. This should include evaluation of PM (AOD), O₃, and radiation (Figures 1, 2, 3, 4). The results of this evaluation (consistency or not with summertime evaluation) should be briefly discussed in the main text.

→ We added evaluation figures for annual means as suggested. The original Fig. S4 shows evaluations of annual carbon fluxes (corresponding to the summer results in Fig. 1). The newly added Fig. S5 shows evaluations of annual AOD, [O₃], and PM_{2.5} concentrations (corresponding to the summer results in Fig. 2). The original Fig. 3 has already included results in non-summer seasons. The newly added Fig. S6 shows evaluations of annual radiation and diffuse fraction (corresponding to the summer results in Fig. 4).

We have revised text properly to refer to these new figures. For example:

Evaluations at rural sites (Table S4) show a mean bias of -5% (Fig. 3). The magnitude of such bias is much lower than the values of comparisons at urban-dominant sites, where simulated [O₃] is higher by 42.5% for the summer mean (Fig. 2f) and 55.6% for the annual mean (Fig. S5f). (Lines 354-357)

Simulated surface shortwave radiation agrees well with measurements at 106 sites for both summer (Figs 4a-4c) and annual (Figs S6a-S6c) means. (Lines 365-367)

Simulated diffuse fraction reproduces observed spatial pattern with high correlation coefficient ($r = 0.74$ for summer and $r = 0.65$ for annual, $p < 0.01$), though it is larger than observations on average by 25.2% in summer (Figs 4d-4f) and 35.2% for the annual mean (Figs S6d-S6f). (Lines 367-370)

4. The paper should discuss the potential implications of the high bias in simulated diffuse fraction and potentially in O₃ (the evaluation of simulated O₃ is mixed).

→ We added following statements to discuss the implications of biases in diffuse fraction and O₃: “Predicted [O₃] is largely overestimated at urban sites but exhibits reasonable magnitude at rural sites (Figs 2 and 3). Measurements of background [O₃] in China are limited both in space and time, restricting comprehensive validation of [O₃] and the consequent estimate of O₃ damages on the country level.” (Lines 595-598)

“The model overestimates diffuse fraction in China (Fig. 4), likely because of simulated biases in clouds. Previously, we improved the prediction of diffuse fraction in China using observed cloud profiles for the region (Yue and Unger, 2017). Biases in simulated AOD and diffuse fraction introduce uncertainties in the aerosol DRF especially in the affected localized model grid cells. Yet, averaged over the China domain, our estimate of NPP change by aerosol DRF (0.09 Pg C yr⁻¹) is consistent with the previous assessment in Yue and Unger (2017) (0.07 Pg C yr⁻¹.” (Lines 619-625)

A follow-up question. As the authors emphasize that rural sites are more appropriate for evaluating their simulation, it seems reasonable to ask what fraction of the GPP change induced by pollution occurs over “urban” gridboxes? They suggest on line 541 that the change in GPP mainly derives from Eastern China, which is largely urban. This would provide some guidance as to how to interpret the relative urban vs rural O3 simulation bias.

→ The reviewer proposed an interesting question. For this study, we use grid resolution of 2°×2.5° latitude by longitude, which is too coarse to identify ‘urban’ gridboxes. However, we can answer the question based on information from ‘China Statistical Yearbook for 2015’ (see the table below). The total urban area in China is 184098.6 km², which is 2% of the total land area. Considering that most of cities are located in eastern part (>1/3 of domestic area), the percentage of urban area should be less than 6% in the east. As a result, we need to evaluate [O₃] at rural areas rather than urban areas, especially when rural concentrations are usually much higher.

In the text, we added the following statistics:

Based on ‘China Statistical Yearbook for 2015’ (<http://www.stats.gov.cn>), the total rural area accounts for >98% of the domestic area. Evaluations at rural sites (Table S4) show a mean bias of -5% (Fig. 3). (Lines 352-354)

25-4 分地区城市建设情况 (2014年)

地区	城区面积 (平方公里)	建成区面积 (平方公里)	城市建设 用地面积 (平方公里)	本年征用 土地面积 (平方公里)	城市人口 密度 (人/平方公里)
全国	184098.6	49772.6	49982.7	1475.9	2419

6. Line 202-203: *do these changes in biomass burning emissions seem realistic?*

→ The reviewer raises an interesting and provocative question. The future changes in biomass burning in China are small, and that is indeed realistic based on current understanding of fire activity in China today. For example, wildfire activity is limited in China today. We state in the manuscript: “Biomass burning emissions, adopted from the IPCC RCP8.5 scenario (van Vuuren et al., 2011), are considered as anthropogenic sources because most fire activities in China are due to human-managed prescribed burning. Compared with the GAINS inventory, present-day biomass burning is equivalent to <1% of the emissions for NO_x, SO₂, and NH₃, 1.6% for BC, 3.0% for

CO, and 9.6% for OC.” (Lines 213-217)

New sentence on fire activity in China being anthropogenic needs a literature reference.

→ We refer to the recent study by Zhou et al. (2017), which compiled a detailed biomass burning emission inventory in China and found that domestic straw burning, in-field straw burning, and firewood burning are the dominant biomass burning sources. In our revised paper, we added the reference as follows:

“Biomass burning emissions, adopted from the IPCC RCP8.5 scenario (van Vuuren et al., 2011), are considered as anthropogenic sources because most fire activities in China are due to human-managed prescribed burning (Zhou et al., 2017).” (Lines 216-218)

Zhou, Y., Xing, X., Lang, J., Chen, D., Cheng, S., Wei, L., Wei, X., and Liu, C.: A comprehensive biomass burning emission inventory with high spatial and temporal resolution in China, *Atmospheric Chemistry and Physics*, 17, 2839-2864, doi:10.5194/acp-17-2839-2017, 2017.

8. Lines 208-209: Please explain why isoprene emissions increase and monoterpene emissions decrease (text later indicates that land cover is fixed) → Please see above response to Point (7).

This is still a little unclear. Is the difference in emissions response for MT and ISOP emission to CO₂, T, GPP (are MT emissions sensitive to GPP?) due to very different sensitivities to these factors, or due to geographical factors (i.e. regions dominated by MT see larger changes in CO₂ than T, etc.)

→ Emissions of isoprene and monoterpene have different sensitivity to CO₂. Increases of CO₂ always inhibit monoterpene but not for isoprene, which is also dependent on photosynthesis that may increase due to CO₂ fertilization. In the revised text, we have explained this clearly:

“Leaf isoprene emissions are simulated using a biochemical model that depends on the electron transport-limited photosynthetic rate, intercellular CO₂, canopy temperature, and atmospheric CO₂ (Unger et al., 2013). Leaf monoterpene emissions depend on canopy temperature and atmospheric CO₂ (Unger and Yue, 2014). Annual average isoprene emission in China increases by 5% (0.39 Tg C yr⁻¹) between 2010 and 2030 in response to enhanced GPP and temperature that offset the effects of CO₂-inhibition. Monoterpene emissions decrease by 5% (-0.25 Tg C) between 2010 and 2030 because CO₂-inhibition outweighs the effects of increased warming.” (Lines 235-242).

12. Section 3.1.2 & Figure 2: Please briefly discuss where the model is too high and too low and what species might contribute to these biases. Also quantify the last sentence (line 298-299) → We

describe the AOD biases as follows: “Predicted AOD also reproduces the observed spatial pattern, but underestimates the high center in NCP by 24.6%.” (Lines 339-340)

In the Discussion Section 4.2, we explain the cause of AOD biases: “Simulated surface PM_{2.5} is reasonable but AOD is underestimated in the North China Plain (Fig. 2), likely because of the biases in aerosol optical parameters. Using a different set of optical parameters, we predicted much higher AOD that is closer to observations with the same aerosol vertical profile and particle compositions (Yue and Unger, 2017).” (Lines 615- 619)

We revise the text as follows: “Evaluations at rural sites (Table S4), which represent the major domain of China, show a mean bias of -5% (Fig. 3). The magnitude of such bias is much lower than the value of 42.5% for the comparisons at urban-dominant sites (Fig.

2f).” (Lines 346-348)

Is there any particular aspect to the “different set of optical parameters” that improves the simulation (i.e. scattering, absorption, water uptake, etc.)? Why did the authors not then use these superior aerosol optical parameters? A description & citation for current optical properties should be added to the Model Description.

→ We use different optical parameters only because it is applied for a different radiation model. Optical parameters used by climate model NASA ModelE2-YIBs have been defined based on previous evaluations on global and regional scales. For this study, we cannot simply revise the parameters because this will affect the energy balance of climate model, resulting in possible overflow of calculation and/or incorrect climatic responses. In the revised paper, we added following description of optical properties:

“Size-dependent optical parameters of clouds and aerosols are computed from Mie scattering, ray tracing, and T-matrix theory, and include the effects of non-spherical particles for cirrus and dust (Schmidt et al., 2006).” (Lines 180-182).

Additional Points

1. Lines 340-341: It’s not clear what this new text means. Was the baseline meteorology adjusted by these scaling factors? For each grid box? Please clarify/expand the description of this procedure.

→ We clarify as follows: “For these simulations, the month-to-month meteorological

perturbations caused by aerosols are applied as scaling factors on the baseline forcing for each month at each grid square.” (Lines 311-313)

2. Lines 360-366: line 360 indicates that NPP and GPP biases are less than 20%, but then specific biases of 23.7%, 20.6%, 40.0%, 51.2%, and 38.7% are not consistent with this. Please correct this text.

→ The bias of <21% is for the evaluations at national scale. As shown in Fig. 1 and Fig. S4, modeling biases are -15.8% for summer GPP, 20.6% for summer NPP, -3.9% for annual GPP, and 12.6% for annual NPP. The biases higher than 20% listed above are for regional scale. In the revised paper, we clarify as follows:

“Simulated GPP and NPP reproduce the observed spatial patterns with high correlation coefficients ($R=0.46-0.86$, $p < 0.001$) and relatively low model-to-observation biases ($\leq 21\%$ on national scale)” (Lines 328-330).

3. Section 3.1.3: The overestimate of diffuse fraction (line 398) seems likely to be associated with clouds (this is stated later in the text) given that aerosols are, if anything, underestimated. Have the authors compared the simulated clouds with other observational datasets? How do MERRA and the online clouds compare?

→ The MERRA cloud fields are reanalyses data based on modeling and may be biased compared with satellite retrievals. Cloud variables and related radiation fields have been thoroughly evaluated in Schmidt et al. (2014). Compared with satellite data, cloud amount is biased by $\pm 5\%$ (which is reasonably low) over eastern China.

Schmidt, G. A., and coauthors: Configuration and assessment of the GISS ModelE2 contributions to the CMIP5 archive, *Journal of Advances in Modeling Earth Systems*, 6, 141-184, doi:10.1002/2013ms000265, 2014.

4. Figures 6, 8, 9, 10: could the authors indicate whether the local results are significant compared to interannual variability (as In Figure 7)

→ We show figures with significant tests in the revised paper. We added dots on Figure 6 to indicate grid squares with significant changes ($p < 0.05$). We replaced Figures 8 and 9

with new ones that only showing significant changes ($p < 0.05$). for Figure 10, the original plot shows only significant changes in (a)-(c) and we did not make further changes.

1 **Ozone and haze pollution weakens net primary productivity in China**

2
3 Xu Yue¹, Nadine Unger², Kandice Harper³, Xiangao Xia⁴, Hong Liao⁵, Tong Zhu⁶,
4 Jingfeng Xiao⁷, Zhaozhong Feng⁸, and Jing Li⁹

5
6 ¹Climate Change Research Center, Institute of Atmospheric Physics, Chinese Academy of
7 Sciences, Beijing 100029, China

8 ²College of Engineering, Mathematics and Physical Sciences, University of Exeter, Exeter,
9 EX4 4QE, UK

10 ³School of Forestry and Environmental Studies, Yale University, 195 Prospect Street, New
11 Haven, Connecticut 06511, USA

12 ⁴Laboratory for Middle Atmosphere and Global Environment Observation, Institute of
13 Atmospheric Physics, Chinese Academy of Sciences, Beijing 100029, China

14 ⁵School of Environmental Science and Engineering, Nanjing University of Information
15 Science & Technology, Nanjing 210044, China

16 ⁶State Key Laboratory for Environmental Simulation and Pollution Control, College of
17 Environmental Sciences and Engineering, Peking University, Beijing 100871, China.

18 ⁷Earth Systems Research Center, Institute for the Study of Earth, Oceans, and Space,
19 University of New Hampshire, Durham, NH 03824, USA

20 ⁸Research Center for Eco-Environmental Sciences, Chinese Academy of Sciences, Beijing
21 100085, China

22 ⁹Laboratory for Climate and Ocean-Atmosphere Studies, Department of Atmospheric and
23 Oceanic Sciences, School of Physics, Peking University, Beijing 100871, China

24
25
26 *Corresponding author:*

27 Xu Yue

28 Telephone: 86-10-82995369

29 Email: xuyueseas@gmail.com

30
31
32 *Keywords:* Haze pollution, climate projection, pollution mitigation, ozone damage, diffuse
33 radiative fertilization, aerosol radiative effects, aerosol indirect effects, photosynthesis, net
34 primary productivity

Abstract

36
37
38
39
40
41
42
43
44
45
46
47
48
49
50
51
52
53
54
55
56
57
58
59
60
61
62
63

Atmospheric pollutants have both beneficial and detrimental effects on carbon uptake by land ecosystems. Surface ozone (O₃) damages leaf photosynthesis by oxidizing plant cells, while aerosols promote carbon uptake by increasing diffuse radiation and exert additional influences through concomitant perturbations to meteorology and hydrology. China is currently the world's largest emitter of both carbon dioxide and short-lived air pollutants. The land ecosystems of China are estimated to provide a carbon sink, but it remains unclear whether air pollution acts to inhibit or promote carbon uptake. Here, we employ Earth system modeling and multiple measurement datasets to assess the separate and combined effects of anthropogenic O₃ and aerosol pollution on net primary productivity (NPP) in China. In the present day, O₃ reduces annual NPP by 0.6 Pg C (14%) with a range from 0.4 Pg C (low O₃ sensitivity) to 0.8 Pg C (high O₃ sensitivity). In contrast, aerosol direct effects increase NPP by 0.2 Pg C (5%) through the combination of diffuse radiation fertilization, reduced canopy temperatures, and reduced evaporation leading to higher soil moisture. Consequently, the net effects of O₃ and aerosols decrease NPP by 0.4 Pg C (9%) with a range from 0.2 Pg C (low O₃ sensitivity) to 0.6 Pg C (high O₃ sensitivity). However, precipitation inhibition from combined aerosol direct and indirect effects reduces annual NPP by 0.2 Pg C (4%), leading to a net air pollution suppression of 0.8 Pg C (16%) with a range from 0.6 Pg C (low O₃ sensitivity) to 1.0 Pg C (high O₃ sensitivity). Our results reveal strong dampening effects of air pollution on the land carbon uptake in China today. Following the current legislation emission scenario, this suppression will be further increased by the year 2030, mainly due to a continuing increase in surface O₃. However, the maximum technically feasible reduction scenario could drastically relieve the current level of NPP damage by 70% in 2030, offering protection of this critical ecosystem service and the mitigation of long-term global warming.

64 **1 Introduction**

65

66 Surface ozone (O₃) and atmospheric aerosols influence land ecosystem carbon uptake both
67 directly and indirectly through Earth system interactions. O₃ reduces plant photosynthesis
68 directly through stomatal uptake. The level of damage is dependent on both surface ozone
69 concentrations ([O₃]) and the stomatal conductance (g_s), the latter of which is closely
70 related to the photosynthetic rate (Reich and Amundson, 1985; Sitch et al., 2007;
71 Ainsworth et al., 2012). The impact of aerosol pollution on vegetation is less clear.
72 Atmospheric aerosols influence plant photosynthesis through perturbations to radiation,
73 meteorology, and clouds. Observations (Cirino et al., 2014; Strada et al., 2015) suggest that
74 an increase in diffuse light partitioning in response to a moderate aerosol loading can
75 improve canopy light use efficiency (LUE) and promote photosynthesis, known as diffuse
76 radiation fertilization (DRF), as long as the total light availability is not compromised
77 (Kanniah et al., 2012). Atmospheric aerosols also reduce leaf temperature (Steiner and
78 Chameides, 2005; Cirino et al., 2014), but the consequence for photosynthesis depends on
79 the relationship between the local environmental temperature and the photosynthetic
80 optimum temperature of approximately 25°C. Aerosol-induced changes in evaporation and
81 precipitation are interconnected but impose opposite effects on photosynthesis; less
82 evaporation preserves soil moisture in the short term but may decrease local rainfall
83 (Spracklen et al., 2012) and lead to drought conditions in the long term. Furthermore,
84 aerosol indirect effects (AIE) on cloud properties can either exacerbate or alleviate the
85 above feedbacks.

86

87 China is currently the world's largest emitter of both carbon dioxide and short-lived air
88 pollutants (<http://gains.iiasa.ac.at/models/>). The land ecosystems of China are estimated to
89 provide a carbon sink (Piao et al., 2009), but it remains unclear how air pollution may affect
90 this sink through the atmospheric influences on regional carbon uptake. O₃ damages to
91 photosynthesis, including those in China, have been quantified in hundreds of
92 measurements (Table S1), but are limited to individual plant species and specific O₃
93 concentrations ([O₃]). Previous regional modeling of O₃ vegetation damage (e.g., Ren et
94 al., 2011; Tian et al., 2011) does not always take advantage of valuable observations to

95 calibrate GPP-O₃ sensitivity coefficients for China domain and typically the derived results
96 have not been properly validated. The aerosol effects on photosynthesis are less well
97 understood. Most of the limited observation-based studies (Rocha et al., 2004; Cirino et
98 al., 2014; Strada et al., 2015) rely on long-term flux measurements or satellite retrievals,
99 which are unable to unravel impacts of changes in the associated meteorological and
100 hydrological forcings. Modeling studies focus mainly on the aerosol-induced enhancement
101 in diffuse radiation (e.g., Cohan et al., 2002; Gu et al., 2003; Mercado et al., 2009), but
102 ignore other direct and indirect feedbacks such as changes in temperature and precipitation.
103 Finally, no studies have investigated the combined effects of O₃ and aerosols or how the
104 air pollution influences may vary in response to future emission regulations and climate
105 change.

106

107 In this study, we assess the impacts of O₃ and aerosols on land carbon uptake in China
108 using the global Earth system model NASA GISS ModelE2 that embeds the Yale
109 Interactive Terrestrial Biosphere model (YIBs). This framework is known as NASA
110 ModelE2-YIBs and fully couples the land carbon-oxidant-aerosol-climate system (Schmidt
111 et al., 2014; Yue and Unger, 2015). The global-scale model accounts for long-range
112 transport of pollution and large-scale feedbacks in physical climate change. The coupled
113 Earth system simulations apply present-day and future pollution emission inventories from
114 the Greenhouse Gas and Air Pollution Interactions and Synergies (GAINS) integrated
115 assessment model (<http://gains.iiasa.ac.at/models/>). The simulations include process-
116 based, mechanistic photosynthetic responses to physical climate change, O₃ stomatal
117 uptake, carbon dioxide (CO₂) fertilization, and aerosol radiative perturbations, but not
118 aerosol and acid deposition (Table 1). The O₃ and aerosol haze effects on the land carbon
119 cycle fluxes occur predominantly through changes to gross primary productivity (GPP) and
120 net primary productivity (NPP). Therefore, the current study focuses on GPP and NPP
121 impacts and does not address changes in net ecosystem exchange (NEE).

122

123 **2 Methods**

124

125 **2.1 YIBs vegetation model**

126

127 The YIBs model applies the well-established Farquhar and Ball-Berry models (Farquhar
128 et al., 1980; Ball et al., 1987) to calculate leaf photosynthesis and stomatal conductance,
129 and adopts a canopy radiation scheme (Spitters, 1986) to separate diffuse and direct light
130 for sunlit and shaded leaves. The assimilated carbon is dynamically allocated and stored to
131 support leaf development (changes in leaf area index, LAI) and tree growth (changes in
132 height). A process-based soil respiration scheme that considers carbon flows among 12
133 biogeochemical pools is included to simulate carbon exchange for the whole ecosystem
134 (Yue and Unger, 2015). Similar to many terrestrial models (Schaefer et al., 2012), the
135 current version of YIBs does not include a dynamic N cycle. Except for this deficit, the
136 vegetation model can reasonably simulate ecosystem responses to changes in [CO₂],
137 meteorology, phenology, and land cover (Yue et al., 2015). A semi-mechanistic O₃
138 vegetation damage scheme (Sitch et al., 2007) is implemented to quantify responses of
139 photosynthesis and stomatal conductance to O₃ (Yue and Unger, 2014).

140

141 The YIBs model can be used in three different configurations: site-level, global/regional
142 offline, and online within ModelE2-YIBs (Yue and Unger, 2015). The offline version is
143 driven with hourly 1°×1° meteorological forcings from either the NASA Modern Era
144 Retrospective-analysis for Research and Applications (MERRA) (Rienecker et al., 2011)
145 or the interpolated output from ModelE2-YIBs. The online YIBs model is coupled with the
146 climate model NASA ModelE2 (Schmidt et al., 2014), which considers the interplay
147 among meteorology, radiation, atmospheric chemistry, and plant photosynthesis at each
148 time step. For both global and regional simulations, 8 plant functional types (PFTs) are
149 considered (Fig. S1). This land cover is aggregated from a dataset with 16 PFTs, which are
150 derived using retrievals from both the Moderate Resolution Imaging Spectroradiometer
151 (MODIS) (Hansen et al., 2003) and the Advanced Very High Resolution Radiometer
152 (AVHRR) (Defries et al., 2000). The same vegetation cover with 16 PFTs is used by the
153 Community Land Model (CLM) (Oleson et al., 2010).

154

155 Both the online and offline YIBs models have been extensively evaluated with site-level
156 measurements from 145 globally-dispersed flux tower sites, long-term gridded benchmark

157 products, and multiple satellite retrievals of LAI, tree height, phenology, and carbon fluxes
158 (Yue and Unger, 2015; Yue et al., 2015). Driven with meteorological reanalyses, the offline
159 YIBs vegetation model estimates a global GPP of $122.3 \pm 3.1 \text{ Pg C yr}^{-1}$, NPP of 63.6 ± 1.9
160 Pg C yr^{-1} , and NEE of $-2.4 \pm 0.7 \text{ Pg C yr}^{-1}$ for 1980-2011, consistent with an ensemble of
161 land models (Yue and Unger, 2015). The online simulations with ModelE2-YIBs,
162 including both aerosol effects and O_3 damage, yield a global GPP of $125.8 \pm 3.1 \text{ Pg C yr}^{-1}$,
163 NPP of $63.2 \pm 0.4 \text{ Pg C yr}^{-1}$, and NEE of $-3.0 \pm 0.4 \text{ Pg C yr}^{-1}$ under present day conditions.
164

165 **2.2 NASA ModelE2-YIBs model**

166

167 The NASA ModelE2-YIBs is a fully coupled chemistry-carbon-climate model with
168 horizontal resolution of $2^\circ \times 2.5^\circ$ latitude by longitude and 40 vertical levels extending to
169 0.1 hPa. The model simulates gas-phase chemistry (NO_x , HO_x , O_x , CO, CH_4 , NMVOCs),
170 aerosols (sulfate, nitrate, elemental and organic carbon, dust, sea salt), and their interactions
171 (Schmidt et al., 2014). Modeled oxidants influence the photochemical formation of
172 secondary aerosol species (sulfate, nitrate, secondary organic aerosol). In turn, modeled
173 aerosols affect photolysis rates in the online gas-phase chemistry (Schmidt et al., 2014).
174 Heterogeneous chemistry on dust surfaces is represented (Bauer et al., 2007). The
175 embedded radiation package includes both direct and indirect (Menon and Rotstajn, 2006)
176 radiative effects of aerosols and considers absorption by multiple GHGs. [Size-dependent
177 optical parameters of clouds and aerosols are computed from Mie scattering, ray tracing,
178 and T-matrix theory, and include the effects of non-spherical particles for cirrus and dust
179 \(Schmidt et al., 2006\).](#) Simulated surface solar radiation exhibits the lowest model-to-
180 observation biases compared with the other 20 IPCC-class climate models (Wild et al.,
181 2013). Simulated meteorological and hydrological variables have been full validated
182 against observations and reanalysis products (Schmidt et al., 2014).
183

184 **2.3 Emissions**

185

186 We use global annual anthropogenic pollution inventories from the GAINS integrated
187 assessment model (Amann et al., 2011), which compiles historic emissions of air pollutants

188 for each country based on available international emission inventories and national
189 information from individual countries. Inter-comparison of present-day (the year 2010)
190 emissions (Fig. S2) shows that the GAINS V4a inventory has similar emission intensity
191 (within $\pm 10\%$) in China as IPCC RCP8.5 scenario (van Vuuren et al., 2011) for most
192 species, except for ammonia, which is higher by 80% in GAINS. The discrepancies among
193 different inventories emerge from varied assumptions on the stringency and effectiveness
194 of emission control measures. While the GAINS 2010 ammonia emissions from China are
195 larger than the RCP8.5 and HTAP emissions as shown in Fig. S2, they are close in
196 magnitude to the year 2010 emissions of 13.84 Tg yr^{-1} estimated by the Regional Emission
197 inventory in ASia (REAS, <http://www.nies.go.jp/REAS/>).

198

199 The GAINS inventory also projects medium-term variations of future emissions at five-
200 year intervals to the year 2030. The current legislation emissions (CLE) scenario applies
201 full implementation of national legislation affecting air pollution emissions; for China, this
202 represents the 11th five-year plan, including known failures. By 2030, in the CLE inventory,
203 CO decreases by 18%, SO₂ by 21%, black carbon (BC) by 28%, and organic carbon (OC)
204 by 41%, but NO_x increases by 20%, ammonia by 22%, and non-methane volatile organic
205 compounds (NMVOC) by 6%, relative to the 2010 emission magnitude in China. To
206 account for potential rapid changes in policy and legislation, we apply the maximum
207 technically feasible reduction (MTFR) emission scenario as the lower limit of future air
208 pollution. The MTFR scenario implements all currently available control technologies,
209 disregarding implementation barriers and costs. With this scenario, the 2030 emissions of
210 NO_x decrease by 76%, CO by 79%, SO₂ by 67%, BC by 81%, OC by 89%, ammonia by
211 65%, and NMVOC by 62% in China, indicating large improvement of air quality. Biomass
212 burning emissions, adopted from the IPCC RCP8.5 scenario (van Vuuren et al., 2011), are
213 considered as anthropogenic sources because most fire activities in China are due to
214 human-managed prescribed burning (Zhou et al., 2017). Compared with the GAINS
215 inventory, present-day biomass burning is equivalent to <1% of the emissions for NO_x,
216 SO₂, and NH₃, 1.6% for BC, 3.0% for CO, and 9.6% for OC. By the year 2030, biomass
217 burning emissions decrease by 1-2% for all pollution species compared with 2010.

218

Deleted: .

220 The model represents climate-sensitive natural precursor emissions of lightning NO_x, soil
221 NO_x and biogenic volatile organic compounds (BVOCs) (Unger and Yue, 2014). Future
222 2030 changes in these natural emissions are small compared to the anthropogenic emission
223 changes. Interactive lightning NO_x emissions are calculated based on the climate model's
224 moist convection scheme that is used to derive the total lightning and the cloud-to-ground
225 lightning frequencies (Price et al., 1997; Pickering et al., 1998; Shindell et al., 2013).
226 Annual average lightning NO_x emissions over China increase by 4% between 2010 and
227 2030. Interactive biogenic soil NO_x emission is parameterized as a function of PFT-type,
228 soil temperature, precipitation (including pulsing events), fertilizer loss, LAI, NO_x dry
229 deposition rate, and canopy wind speed (Yienger and Levy, 1995). Annual average
230 biogenic soil NO_x emissions increase by only 1% over China between 2010 and 2030. Leaf
231 isoprene emissions are simulated using a biochemical model that depends on the electron
232 transport-limited photosynthetic rate, intercellular CO₂, canopy temperature, and
233 atmospheric CO₂ (Unger et al., 2013). Leaf monoterpene emissions depend on canopy
234 temperature and atmospheric CO₂ (Unger and Yue, 2014). Annual average isoprene
235 emission in China increases by 5% (0.39 Tg C yr⁻¹) between 2010 and 2030 in response to
236 enhanced GPP and temperature that offset the effects of CO₂-inhibition. Monoterpene
237 emissions decrease by 5% (-0.25 Tg C) between 2010 and 2030 because CO₂-inhibition
238 outweighs the effects of increased warming.

239

240 **2.4 Simulations**

241

242 **2.4.1 NASA ModelE2-YIBs online**

243 We perform 24 time-slice simulations to explore the interactive impacts of O₃ and aerosols
244 on land carbon uptake (Table 2). All simulations are performed in atmosphere-only
245 configuration. In these experiments, [O₃] and aerosol loading are dynamically predicted,
246 and atmospheric chemistry processes are fully two-way coupled to the meteorology and
247 the land biosphere. Simulations can be divided into two groups, depending on whether AIE
248 are included. In each group, three subgroups are defined with the emission inventories of
249 GAINS 2010, CLE 2030, and MTRF 2030 scenarios. In each subgroup, one baseline
250 experiment is set up with only natural emissions (denoted with NAT). The other three

251 implement all natural and anthropogenic sources of emissions (denoted with ALL), but
252 apply different levels of O₃ damage including none (denoted with NO3), low sensitivity
253 (LO3), and high sensitivity (HO3). To compare the differences between online and offline
254 O₃ damage, we perform four additional simulations which do not account for the feedbacks
255 of O₃-induced changes in biometeorology, plant growth, and ecosystem physiology. Two
256 simulations, G10ALLHO3_OFF and G10ALLLO3_OFF, include both natural and
257 anthropogenic emissions. The other two, G10NATHO3_OFF and G10NATLO3_OFF,
258 include natural emissions alone.

259

260 We use prescribed sea surface temperature (SST) and sea ice distributions simulated by
261 ModelE2 under the IPCC RCP8.5 scenario (van Vuuren et al., 2011). For these boundary
262 conditions, we apply the monthly-varying decadal average of 2006-2015 for 2010
263 simulations and that of 2026-2035 for 2030 simulations. Well-mixed GHG concentrations
264 are also adopted from the RCP8.5 scenario, with CO₂ changes from 390 ppm in 2010 to
265 449 ppm in 2030, and CH₄ changes from 1.779 ppm to 2.132 ppm. Land cover change
266 projections for this scenario suggest only minor changes between the years 2010 and 2030;
267 for example, the expansion of 3% for grassland is offset by the losses of 1% for cropland
268 and 4% for tropical rainforest. As a result, we elect to apply the same land cover, which is
269 derived from satellite retrievals, for both present-day and future simulations (Fig. S1). We
270 use present-day equilibrium tree height derived from a 30-year spinup procedure (Yue and
271 Unger, 2015) as the initial condition. All simulations are performed for 20 years, and the
272 last 15 years are used for analyses. For simulations including effects of CO₂ fertilization,
273 climate change, and O₃ damages, GPP and NPP reach new equilibrium within 5 years while
274 those for NEE may require several decades due to the slow responses of the soil carbon
275 pools (Fig. S3). The full list of simulations in Table 2 offers assessment of uncertainties
276 due to interannual climate variability, emission inventories (CLE or MTRF), O₃ damage
277 sensitivities (low to high), and aerosol climatic effects (direct and indirect). Uncertainties
278 calculated based on the interannual climate variability in the model are indicated using the
279 format 'mean ± one standard deviation'. Other sources of uncertainty are explicitly stated.

280

281 **2.4.2 YIBs offline with MERRA meteorology**

282 We perform 15 simulations to evaluate the skill of the O₃ damage scheme for vegetation in
283 China (Table S2). Each run is driven with hourly meteorological forcings from NASA
284 GMAO MERRA (Rienecker et al., 2011). One baseline simulation is performed without
285 inclusion of any O₃ damage. The others, seven runs in each of two groups, are driven with
286 fixed [O₃] at 20, 40, 60, 80, 100, 120, and 140 ppbv, respectively, using either low or high
287 O₃ sensitivities defined by (Sitch et al., 2007). Thus, [O₃] in these offline runs is fixed
288 without seasonal and diurnal variations to mimic field experiments that usually apply a
289 constant level of [O₃] during the test period. We compare the O₃-affected GPP with the O₃-
290 free GPP from the baseline simulation to derive the damaging percentages to GPP, which
291 are compared with values for different PFTs from an ensemble of published literature
292 results (Table S1). All simulations are performed for 1995-2011, and the last 10 years are
293 used for analyses.

294

295 **2.4.3 YIBs offline with ModelE2-YIBs meteorology**

296 Using the offline YIBs vegetation model driven with ModelE2-YIBs meteorology, we
297 perform 30 simulations to isolate the impacts of aerosol-induced changes in the individual
298 meteorological drivers on carbon uptake (Table S3). Experiments are categorized into two
299 groups, depending on whether the GCM forcings include AIE or not. In each group, three
300 subgroups of simulations are set up with different meteorology for GAINS 2010, CLE
301 2030, and MTRF 2030 scenarios. Within each subgroup, five runs are designed with the
302 different combinations of GCM forcings. One baseline run is forced with meteorology
303 simulated without anthropogenic aerosols. The other four are additionally driven with
304 aerosol-induced perturbations in temperature, PAR, soil moisture, or the combination of
305 the above three variables. For these simulations, the month-to-month meteorological
306 perturbations caused by aerosols are applied as scaling factors on the baseline forcing for
307 each month at each grid square. The differences of NPP between sensitivity and baseline
308 runs represent contributions of individual or total aerosol effects. Each simulation is
309 performed for 15 years, with the last 10 years used for analyses. Uncertainties due to
310 interannual climate variability in the model are calculated using different time periods for
311 the online (15 years, Table 2) and offline (10 years, Table S3) runs.

312

Deleted: .

314 3 Results

315

316 3.1 Evaluation of ModelE2-YIBs over China

317

318 3.1.1 Land carbon fluxes: GPP and NPP

319 To validate simulated GPP, we use a gridded benchmark product for 2009-2011 upscaled
320 from *in situ* FLUXNET measurements (Jung et al., 2009). For NPP, we use a MODIS
321 satellite-derived product for 2009-2011 (Zhao et al., 2005). Both datasets are interpolated
322 to the same resolution of $2^\circ \times 2.5^\circ$ as ModelE2-YIBs. Simulated GPP and NPP reproduce
323 the observed spatial patterns with high correlation coefficients ($R=0.46-0.86$, $p < 0.001$)
324 and relatively low model-to-observation biases ($< 21\%$ on national scale) (Fig. 1 and Fig.
325 S4). High values of the land carbon fluxes are predicted in the East and the Northeast,
326 where forests and croplands dominate (Fig. S1). For GPP, prediction in the summer
327 overestimates by 6.2% over the southern coast ($< 28^\circ\text{N}$), but underestimates by 23.7% over
328 the North China Plain (NCP, $[32-40^\circ\text{N}, 110-120^\circ\text{E}]$). Compared with the MODIS data
329 product, predicted summer NPP is overall overestimated by 20.6% in China (Fig. 1f), with
330 regional biases of 40.0% in the southern coast, 51.2% in the NCP, and 38.7% in the
331 Northeast ($> 124^\circ\text{E}$).

332

333 3.1.2 Surface air pollution and AOD

334 For surface concentrations of $\text{PM}_{2.5}$ and O_3 , we use ground measurements available for
335 2014 from 188 sites operated by the Ministry of Environmental Protection of China
336 (<http://www.aqicn.org/>). In addition, we use rural $[\text{O}_3]$ from published literature (Table S4)
337 to evaluate the model. For AOD, we use gridded observations of 2008-2012 from MODIS
338 retrievals. The model simulates reasonable magnitude and spatial distribution of surface
339 $\text{PM}_{2.5}$ concentrations (Fig. 2 and Fig. S5). Predicted AOD also reproduces the observed
340 spatial pattern, but underestimates the high center in NCP by 24.6% in summer. Long-term
341 measurements of $[\text{O}_3]$ are very limited in China. Comparisons with the 2014 one-year data
342 from 188 urban sites show that simulated $[\text{O}_3]$ reproduces reasonable spatial distribution
343 but overestimates the average concentration by $>40\%$ (Fig. 2f and Fig. S5f). Such
344 discrepancy is in part attributed to the sampling biases, because urban $[\text{O}_3]$ is likely lower

Deleted: 20%

Deleted: %.

Deleted: %.

348 than rural [O₃] due to high NO_x emissions (NO_x titration) and aerosol loading (light
349 extinction) in cities. Based on 'China Statistical Yearbook for 2015'
350 (<http://www.stats.gov.cn>), the total rural area accounts for >98% of the domestic area.
351 Evaluations at rural sites (Table S4) show a mean bias of -5% (Fig. 3). The magnitude of
352 such bias is much lower than the values of comparisons at urban-dominant sites, where
353 simulated [O₃] is higher by 42.5% for the summer mean (Fig. 2f) and 55.6% for the annual
354 mean (Fig. S5f).

Deleted:), which represent the major domain of China,
Deleted: value
Deleted: 42.5% for the
Deleted:).

355 356 3.1.3 Shortwave radiation

357 We use ground-based observations of surface shortwave radiation and diffuse fraction from
358 106 pyranometer sites managed by the Climate Data Center, Chinese Meteorological
359 Administration (Xia, 2010). Site selection is based on the availability of continuous
360 monthly measurements during 2008-2012, resulting in 95 sites for the evaluation of total
361 shortwave radiation. For diffuse radiation, we select the 17 sites only that provide
362 continuous measurements during 2008-2012. Simulated surface shortwave radiation agrees
363 well with measurements at 106 sites for both summer (Figs 4a-4c) and annual (Figs S6a-
364 S6c) means. Simulated diffuse fraction reproduces observed spatial pattern with high
365 correlation coefficient ($r = 0.74$ for summer and $r = 0.65$ for annual, $p < 0.01$), though it is
366 larger than observations on average by 25.2% in summer (Figs 4d-4f) and 35.2% for the
367 annual mean (Figs S6d-S6f). Such bias is mainly attributed to the overestimation in the
368 North and Northeast. For the southeastern region, where high values of GPP dominate (Fig.
369 1), predicted diffuse fraction is in general within the 10% difference from the observations.

Deleted:).

Deleted: on average 25.2%

370 371 3.1.4 Ozone vegetation damage function

372 We adopt the same approach as Yue et al. (2016) by comparing simulated GPP-to-[O₃]
373 responses (Table S2) with observations from multiple published literature (Table S1). We
374 aggregate these measurements into six categories, including evergreen needleleaf forest
375 (ENF), deciduous broadleaf forest (DBF), shrubland, C3 herbs, C4 herbs, and a mixture of
376 all above species. We derive the sensitivity of GPP to varied [O₃] (Fig. 5) using the YIBs
377 offline version. For most PFTs, simulated O₃ damage increases with [O₃] in broad
378 agreement with measurements. Predicted O₃ damage reproduces observations with a

385 correlation coefficient of 0.61 (for all samplings, $n=32$) and in similar magnitudes (-17.7%
386 vs. -20.4%), suggesting that the damage scheme we adopted from Sitch et al. (2007) is
387 ready to use in China. For the same level of $[O_3]$, deciduous trees suffer larger damages
388 than evergreen trees because the former species are usually more sensitive (Sitch et al.,
389 2007) and have higher g_s (therefore higher uptake) (Wittig et al., 2007). Flux-based O_3
390 sensitivity for C4 herbs is only half that of C3 herbs (Sitch et al., 2007), however,
391 concentration-based O_3 damages, both observed and simulated, are larger for C4 plants
392 because of their higher uptake efficiency following high g_s (Yue and Unger, 2014).

393

394 3.2 O_3 effects in China

395

396 We focus our study domain in eastern China (21°-38°N, 102°-122°E, including the North
397 China Plain, the Yangtze River Delta, and part of the Sichuan Basin), a region that suffers
398 from high levels of O_3 and aerosols from anthropogenic pollution sources (>75%
399 contribution; Fig. S7). We estimate that surface O_3 decreases annual GPP in China by
400 10.3% based on YIBs offline simulations in the absence of feedbacks from O_3 vegetation
401 damage to meteorology and plant growth. The damage is stronger in summer, when the
402 average GPP decreases by ~20% for both deciduous trees and C3 herbs in the East (Fig.
403 6). In contrast, a lower average damage to GPP of ~10% is predicted for evergreen
404 needleleaf trees (because of low sensitivity) and C4 herbs (because of the mismatched
405 spatial locations between C4 plants and high $[O_3]$, Fig. S1 and Fig. 2d).

406

407 O_3 damage to photosynthesis can influence plant growth. At the same time, the O_3 -induced
408 reductions in stomatal conductance (Fig. S8a) can increase canopy temperature and inhibit
409 plant transpiration, leading to surface warming (Fig. S8b), dry air (Fig. S8c), and rainfall
410 deficit (Fig. S8d). These biometeorological feedbacks may in turn exacerbate the
411 dampening of land carbon uptake. Application of ModelE2-YIBs that allows for these
412 feedbacks gives an O_3 -induced damage to annual GPP of 10.7%, a similar level to the
413 damage computed in YIBs offline. The spatial pattern of the online O_3 inhibition also
414 resembles that of offline damages (not shown). Sensitivity simulations with zero
415 anthropogenic emissions show almost no O_3 damage (Fig. S9), because the $[O_3]$ exposure

Deleted: S5

Deleted: S6a

Deleted: S6b

Deleted: S6c

Deleted: S6d

Deleted: S7

422 from natural sources alone is usually lower than the threshold level of 40 ppbv below which
423 the damage for most PFTs is limited (Fig. 5). Our results indicate that present-day surface
424 O₃ causes strong inhibitions on total NPP in China, ranging from 0.43 ± 0.12 Pg C yr⁻¹ with
425 low sensitivity to 0.76 ± 0.15 Pg C yr⁻¹ with high sensitivity (Table 3). The central value
426 of NPP reduction by O₃ is 0.59 ± 0.11 Pg C yr⁻¹, assuming no direct impacts of O₃ on plant
427 respiration. About 61% of such inhibition occurs in summer, when both photosynthesis
428 and [O₃] reach maximum of the year.

429

430 3.3 Aerosol haze effects in China

431

432 Aerosols decrease direct solar radiation but increase diffuse radiation (Fig. S10), the latter
433 of which is beneficial for canopy photosynthesis. The online-coupled model quantifies the
434 concomitant meteorological and hydrological feedbacks (Fig. 7) that further influence the
435 radiative and land carbon fluxes. Reduced insolation decreases summer surface
436 temperature by 0.63°C in the East, inhibiting evaporation but increasing relative humidity
437 (RH) due to the lower saturation vapor pressure (Table S5). These feedbacks combine to
438 stimulate photosynthesis (Fig. 8a), which, in turn, strengthens plant transpiration (not
439 shown). Atmospheric circulation and moisture convergence are also altered due to the
440 pollution-vegetation-climate interactions, resulting in enhanced precipitation (Fig. 7b) and
441 cloud cover (Fig. 7d). Moreover, soil moisture increases (Fig. 7f) with lower evaporation
442 (Fig. 7e) and higher precipitation (Fig. 7b). Inclusion of AIE results in distinct climatic
443 feedbacks (Fig. S11). Summer precipitation decreases by 0.9 mm day⁻¹ (13%), leading to
444 a 3% decline in soil moisture (Table S6). The AIE lengthens cloud lifetime and increases
445 cloud cover, further reducing available radiation and causing a stronger surface cooling.
446 Compared to aerosol-induced perturbations in radiation and temperature, responses in
447 hydrological variables (e.g. precipitation and soil moisture) are usually statistically
448 insignificant on the domain average due to the large relative interannual climate variability
449 (Tables S5 and S6). The resulting meteorological changes over China are a combination of
450 locally driven effects (such as changes in radiation and hence temperature) and regional-
451 globally driven effects (such as changes in rainfall and hence soil water).

452

Deleted: S8

Deleted: S9

455 We separate the relative impacts due to aerosol-induced perturbations in temperature,
456 radiation, and soil moisture (Fig. 8). The overall impact of the aerosol-induced
457 biometeorological feedbacks on the carbon uptake depends on the season and vegetation
458 type. In the summer, the aerosol-induced surface cooling brings leaf temperature closer to
459 the photosynthetic optimum of 25°C, DRF enhances light availability of shaded leaves and
460 LUE of sunlit leaves, and the wetter soil alleviates water stress for stoma. Consequently,
461 aerosol-induced hydroclimatic feedbacks promote ecosystem NPP, albeit with substantial
462 spatiotemporal variability (Fig. 8a and Table 3). Surface cooling enhances NPP in summer
463 (Fig. 8b) but induces neutral net impacts on NPP in spring and autumn (not shown), when
464 leaf temperature is usually below 25°C, because the cooling-driven reductions of
465 photosynthesis are accompanied by simultaneous reductions in plant respiration. We find
466 strong aerosol DRF in the Southeast and the Northeast, where AOD is moderate (Fig. 8c).
467 Over the North China Plain and the Southwest, aerosol DRF is more limited. In these
468 regions, the local background aerosol layer and/or cloud over are sufficiently optically
469 thick that the effect of anthropogenic aerosol pollution is largely to attenuate direct sunlight
470 and reduce NPP (Cohan et al., 2002). Aerosol-induced cooling increases soil moisture over
471 most of the East (Fig. 7f), but the beneficial responses are confined to the Central East (Fig.
472 8d), where C3 crops dominate (Fig. S1). These short-root plants are more sensitive to short-
473 term water availability than deep-root trees (Beer et al., 2010; Yue et al., 2015).

474
475 In contrast, inclusion of AIE results in detrimental impacts on NPP (Table 3). Aerosol-
476 induced drought strongly reduces regional NPP especially over the Northeast and North
477 China Plain (Fig. S12d), where cropland dominates (Fig. S1). Meanwhile, the increases in
478 cloud cover reduce available radiation, leading to weakened aerosol DRF effects over the
479 Southeast while strengthened NPP reductions in the Southwest (Fig. S12c).

Deleted: S10d

Deleted: S10c

481 3.4 Combined effects of O₃ and aerosol

482
483 Simultaneous inclusion of the aerosol effects on the land biosphere has negligible impacts
484 on O₃ damage. The online O₃ inhibition, which is much stronger in magnitude than the
485 aerosol effects, shows insignificant differences relative to the offline values (10.7% vs.

488 10.3%). As a result, we consider O₃ and aerosol effects to be linearly additive. In the year
489 2010, the combined effects of O₃ and aerosols (Table 3) decrease total NPP in China by
490 0.39 (without AIE) to 0.80 Pg C yr⁻¹ (with AIE), equivalent to 9-16% of the pollution-free
491 NPP and 16-32% of the total anthropogenic carbon emissions (Liu et al., 2015). Spatially,
492 a dominant fraction (86% without AIE and 77% with AIE) of the reduced carbon uptake
493 occurs in the East, where dense air pollution is co-located with high NPP (Figs 1 and 2).
494 Temporally, a dominant fraction (60% without AIE and 52% with AIE) of the reduced
495 carbon uptake occurs in summer, when both NPP and [O₃] reach maximum of the year.
496 Independently, O₃ reduces NPP by 0.59 Pg C yr⁻¹, with a large range from 0.43 Pg C yr⁻¹
497 for low damaging sensitivity to 0.76 Pg C yr⁻¹ for high damaging sensitivity (Table 3). The
498 sign of the aerosol effects is uncertain. Without AIE, aerosol is predicted to increase NPP
499 by 0.2 Pg C yr⁻¹, because of regionally confined DRF effects and enhanced soil moisture
500 (Fig. 8). With inclusion of AIE, aerosol decreases NPP by 0.2 Pg C yr⁻¹, mainly due to
501 reduced soil moisture (Fig. S12). The uncertainty of individual simulations, calculated
502 from the interannual climate variability, is usually smaller than that due to O₃ damage
503 sensitivity and AIE (Table 3).

Deleted: S10

504

505 3.5 Future projection of pollution effects

506

507 Following the CLE scenario, by the year 2030, predicted summer [O₃] increases by 7%,
508 while AOD decreases by 5% and surface PM_{2.5} concentrations decline by 10% (Fig. 9).
509 These changes are predominantly attributed to changes in anthropogenic emissions, as
510 natural sources show limited changes. The reduction of AOD is related to the decreased
511 emissions of SO₂, black carbon, and organic carbon (Fig. S2). In contrast, the enhancement
512 of [O₃] results from the increased NO_x emissions, higher level of background CH₄ (~20%),
513 and higher air temperature in the warmer 2030 climate. The moderate decline of aerosol
514 loading in the 2030 CLE scenario brings benefits to land ecosystems through DRF effects
515 (Table 3) because light scattering is often saturated in the present-day conditions due to
516 high local AOD and regional cloud cover. Benefits from the aerosol pollution reductions
517 are offset by worsening O₃ vegetation damage in the CLE future world (Fig. 10b). O₃-free
518 ([O₃]=0) NPP increases by 14% in 2030 due to CO₂ fertilization and global climate change.

520 Despite [CO₂] increases from 390 ppm in 2010 to 449 ppm in 2030 in the RCP8.5 scenario
521 (van Vuuren et al., 2011), which contributes to g_s inhibition of 4% on the country level, the
522 future O₃-induced NPP damage in 2030 degrades to 14% or 0.67 Pg C yr⁻¹ (Table 3), with
523 a range from 0.43 Pg C yr⁻¹ (low O₃ sensitivity) to 0.90 Pg C yr⁻¹ (high O₃ sensitivity).

524

525 The MTRF scenario reflects an ambitious and optimistic future in which there is rapid
526 global implementation of all currently available technological pollution controls. AOD
527 decreases by 55% and [O₃] decreases by 40% for this future scenario (Fig. 9). The model
528 projects much lower damage to NPP of only 0.12 Pg C yr⁻¹, with a range from 0.06 Pg C
529 yr⁻¹ (low O₃ sensitivity) to 0.20 Pg C yr⁻¹ (high O₃ sensitivity), mainly due to the 40%
530 reduction in [O₃] (Fig. 10c). Including both aerosol direct and indirect effects, O₃ and
531 aerosols together inhibit future NPP by 0.28 Pg C yr⁻¹, ranging from 0.12 Pg C yr⁻¹ with
532 low O₃ sensitivity to 0.43 Pg C yr⁻¹ with high O₃ sensitivity. As a result, The MTRF
533 scenario offers strong recovery of the land carbon uptake in China by 2030.

534

535 **4. Discussion**

536

537 **4.1 Comparison with previous estimates**

538

539 Previous estimates of O₃ damages over the whole China region are very limited. Two
540 important studies, Tian et al. (2011) and Ren et al. (2011), have quantified the impacts of
541 surface O₃ on carbon assimilation in China. Both studies applied the dynamic land
542 ecosystem model (DLEM) with O₃ damage scheme proposed by Felzer et al. (2004), except
543 that Tian et al. (2011) focused on NEE while Ren et al. (2011) also investigated NPP. The
544 Felzer et al. (2004) scheme calculates O₃ uptake based on stomatal conductance and the
545 AOT40 (accumulated hourly O₃ dose over a threshold of 40 ppb). Yue and Unger (2014)
546 estimated O₃-induced reductions in GPP over U.S. using Sitch et al. (2007) scheme and
547 found an average value of 4-8% (low to high sensitivity), consistent with the reduction of
548 3-7% in Felzer et al. (2004). For this study, we estimate that present-day O₃ decreases NPP
549 by 0.43-0.76 Pg C yr⁻¹, higher than the 0.42 Pg C yr⁻¹ calculated by Ren et al. (2011).
550 However, the percentage reduction of 10.1-17.8% in our estimate is weaker than the value

551 of 24.7% in Ren et al. (2011). The main reason for such discrepancy lies in the differences
552 in the climatological NPP. Combining all environmental drivers (e.g. [CO₂], meteorology,
553 [O₃], and aerosols), we predict an average NPP of 3.98 ± 0.1 Pg C yr⁻¹ for the year 2010
554 (uncertainties from AIE) with the ModelE2-YIBs model. This value is close to the average
555 of 3.35 ± 1.25 Pg C yr⁻¹ for 1981-2000 calculated based on 54 estimates from 33 studies
556 (Shao et al., 2016). Using DLEM, Ren et al. (2011) estimated an optimal NPP of 1.67 Pg
557 C yr⁻¹ for 2000-2005 over China, which is only half of the literature-based estimate.

558

559 In the absence of any previous studies of aerosol pollution effects on land carbon uptake in
560 China, our strategy is to compare separately the simulated aerosol climatic feedback
561 (climate sensitivity) and simulated NPP response to climate variability (NPP sensitivity)
562 with existing published results. ModelE2-YIBs simulates an annual reduction of 26.2 W
563 m⁻² in all-sky surface solar radiation over the East due to aerosols pollution (Table S5),
564 similar to the estimate of 28 W m⁻² by Folini and Wild (2015). In response to this radiative
565 perturbation, aerosol pollution causes a widespread cooling of 0.3-0.9 °C in summer over
566 the East (Fig. 7a), consistent with estimates of 0-0.9 °C by Qian et al. (2003), 0-0.7 °C by
567 Liu et al. (2009), and average of 0.5 °C by Folini and Wild (2015). Aerosol pollution effects
568 on regional precipitation patterns in China are not well understood due to different climate
569 model treatments of land-atmosphere interactions and the interplay between regional and
570 large-scale circulation. In ModelE2-YIBs, without AIE, aerosol induces a “northern
571 drought and southern flood” pattern in agreement with Gu et al. (2006), but different to Liu
572 et al. (2009) who predicted widespread drought instead. Including both aerosol direct and
573 indirect effects, ModelE2-YIBs simulates an average reduction of 0.48 mm day⁻¹ in
574 summer rainfall widespread over China (Fig. S11b), similar to the magnitude of 0.4 mm
575 day⁻¹ estimated with the ECHAM5-HAM model (Folini and Wild, 2015), but higher than
576 the 0.21 mm day⁻¹ predicted by the RegCM2 model (Huang et al., 2007).

577

578 Sensitivity experiments with YIBs show that summer NPP increases following aerosol-
579 induced changes in temperature, radiation, and precipitation (Fig. 8). The cooling-related
580 NPP enhancement (Fig. 8b) collocates with changes in temperature (Fig. 7a), indicating
581 that sensitivity of NPP to temperature is negative over eastern China. Such temperature

Deleted: S9b

583 sensitivity is consistent with the ensemble estimate based on 10 terrestrial models (Piao et
584 al., 2013). For the aerosol-induced radiative perturbation, many studies have shown that
585 moderate aerosol/cloud amount promotes plant photosynthesis through enhanced DRF,
586 while dense aerosol/cloud decreases carbon uptake due to light extinction (Cohan et al.,
587 2002; Gu et al., 2003; Rocha et al., 2004; Alton, 2008; Knohl and Baldocchi, 2008;
588 Mercado et al., 2009; Jing et al., 2010; Bai et al., 2012; Cirino et al., 2014; Strada et al.,
589 2015). Theoretically, at each specific land location on the Earth, there is an AOD threshold
590 below which aerosol promotes local NPP. The threshold is dependent on latitude,
591 cloud/aerosol amount, and plant types. In a related study by Yue and Unger (2017), we
592 applied a well-validated offline radiation model to calculate these AOD thresholds over
593 China. We conclude that present-day AOD is lower than the local thresholds in the
594 Northeast and Southeast but exceeds the thresholds in the North China Plain, explaining
595 why aerosol-induced dimming enhances NPP in the former regions but reduces NPP in the
596 latter (Fig. 8c). On the country level, the NPP enhancement due to aerosol DRF is 0.07 Pg
597 C yr⁻¹ in Yue and Unger (2017), very close to the 0.09 Pg C yr⁻¹ estimated with ModelE2-
598 YIBs model (Table 2).

599

600 4.2 Uncertainties

601

602 A major source of uncertainty originates from the paucity of observations. For instance,
603 direct measurements of aerosol pollution effects on NPP are non-existent for China. The
604 aerosol effects involve complex interactions that challenge the field-based validation of the
605 underlying independent processes. Field experiments of O₃ vegetation damage are
606 becoming more available, but their applications are limited by the large variations in the
607 species-specific responses (Lombardozi et al., 2013), as well as the discrepancies in the
608 treatments of [O₃] enhancement (Wittig et al., 2007). Instead of equally using all individual
609 records from multiple literatures (Lombardozi et al., 2013), we aggregate O₃ damage for
610 each literature based on the seasonal (or growth-season) average. In this way, the derived
611 PFT-level GPP-[O₃] relationships are not biased towards the experiments with a large
612 number of samplings. Such aggregation also reduces sampling noise and allows
613 construction of the quantified GPP-[O₃] relationships used for model assessment. Predicted

614 [O₃] is largely overestimated at urban sites but exhibits reasonable magnitude at rural sites
615 (Figs 2 and 3). Measurements of background [O₃] in China are limited both in space and
616 time, restricting comprehensive validation of [O₃] and the consequent estimate of O₃
617 damages on the country level.

618

619 We have estimated O₃ damages to NPP (instead of GPP), an optimal indicator for net
620 carbon uptake by plants. Our calculations assume no impacts of O₃ on autotrophic
621 respiration. Yet, limited observations have found increased plant respiration in response to
622 O₃ injury (Felzer et al., 2007), suggesting that our calculation of O₃-induced NPP
623 reductions might be underestimated. Current large mechanistic uncertainties in the role of
624 anthropogenic nitrogen (N) deposition to China's land carbon uptake (Tian et al., 2011;
625 Xiao et al., 2015) have prohibited the inclusion of dynamic carbon-nitrogen coupling in
626 the Earth system model used here. Previous studies have suggested that inclusion of N
627 fertilization can relieve or offset damages by O₃, especially for N-limited forests (Ollinger
628 et al., 2002). Relative to the present day, atmospheric reactive N deposition increases by
629 20% in the CLE scenario but decreases by 60% in the MTFR scenario, suggesting that the
630 stronger O₃ damage in CLE might be overestimated while the reduced damage in MTFR
631 might be too optimistic.

632

633 Our estimate of NPP responses to aerosol pollution is sensitive to modeling uncertainties
634 in concentration, radiation, and climatic effects. Simulated surface PM_{2.5} is reasonable but
635 AOD is underestimated in the North China Plain (Fig. 2), likely because of the biases in
636 aerosol optical parameters. Using a different set of optical parameters, we predicted much
637 higher AOD that is closer to observations with the same aerosol vertical profile and particle
638 compositions (Yue and Unger, 2017). The model overestimates diffuse fraction in China
639 (Fig. 4), likely because of simulated biases in clouds. Previously, we improved the
640 prediction of diffuse fraction in China using observed cloud profiles for the region (Yue
641 and Unger, 2017). Biases in simulated AOD and diffuse fraction introduce uncertainties in
642 the aerosol DRF especially in the affected localized model grid cells. Yet, averaged over
643 the China domain, our estimate of NPP change by aerosol DRF (0.09 Pg C yr⁻¹) is
644 consistent with the previous assessment in Yue and Unger (2017) (0.07 Pg C yr⁻¹). Aerosol-

645 induced impacts on precipitation and soil moisture are not statistically significant over the
646 regionally averaged domain (Tables S5 and S6). However, for the 2010 and 2030 CLE
647 cases with AIE, 2 out of 6 scenarios, the aerosol-induced impact on soil moisture dominates
648 the total NPP response (Table 3). Furthermore, the relatively coarse resolution of the global
649 model and usage of emission inventories may introduce additional biases and exacerbate
650 the total uncertainties.

651
652 Importantly, our estimate of NPP response to aerosol effects, with or without AIE, is
653 secondary in magnitude compared to the O₃ vegetation damage, suggesting that the net
654 impact of current air pollution levels in China is detrimental to the land carbon uptake
655 there. Locally, this pollution damage exerts a threat to plant health, terrestrial ecosystem
656 services, and food production. Globally, air pollution effects may enhance planetary
657 warming by decreasing the land removal rate of atmospheric CO₂. Our results show
658 substantial benefits to the protection of plant health and the regional land carbon sink in
659 China from stringent air pollution controls, especially for O₃ precursors. Our analysis
660 highlights the complex interplay between immediate and more local pollution issues, and
661 longer-term global warming. Future air pollution controls provide an additional co-benefit
662 to human society: the offsetting of fossil fuel CO₂ emissions through enhanced land
663 sequestration of atmospheric CO₂.

664
665 *Acknowledgements.* The authors are grateful to Prof. William Collins and an anonymous
666 reviewer for constructive comments improving this paper. X. Yue acknowledges funding
667 support from the National Basic Research Program of China (973 program, Grant No.
668 2014CB441202) and the “Thousand Youth Talents Plan”. This research was supported in
669 part by the facilities and staff of the Yale University Faculty of Arts and Sciences High
670 Performance Computing Center.

671
672

673 **References**

- 674 Ainsworth, E. A., Yendrek, C. R., Sitch, S., Collins, W. J., and Emberson, L. D.: The
675 Effects of Tropospheric Ozone on Net Primary Productivity and Implications for
676 Climate Change, *Annual Review of Plant Biology*, Vol 63, 63, 637-661,
677 doi:10.1146/Annurev-Arplant-042110-103829, 2012.
- 678 Alton, P. B.: Reduced carbon sequestration in terrestrial ecosystems under overcast skies
679 compared to clear skies, *Agricultural and Forest Meteorology*, 148, 1641–1653,
680 doi:10.1016/j.agrformet.2008.05.014, 2008.
- 681 Amann, M., Bertok, I., Borcken-Kleefeld, J., Cofala, J., Heyes, C., Hoglund-Isaksson, L.,
682 Klimont, Z., Nguyen, B., Posch, M., Rafaj, P., Sandler, R., Schopp, W., Wagner, F.,
683 and Winiwarter, W.: Cost-effective control of air quality and greenhouse gases in
684 Europe: Modeling and policy applications, *Environmental Modelling & Software*, 26,
685 1489-1501, doi:10.1016/j.envsoft.2011.07.012, 2011.
- 686 Bai, Y., Wang, J., Zhang, B., Zhang, Z., and Liang, J.: Comparing the impact of cloudiness
687 on carbon dioxide exchange in a grassland and a maize cropland in northwestern
688 China, *Ecological Research*, 27, 615-623, doi:10.1007/s11284-012-0930-z, 2012.
- 689 Ball, J. T., Woodrow, I. E., and Berry, J. A.: A model predicting stomatal conductance and
690 its contribution to the control of photosynthesis under different environmental
691 conditions, in: *Progress in Photosynthesis Research*, edited by: Biggins, J., Nijhoff,
692 Dordrecht, Netherlands, 110–112, 1987.
- 693 Bauer, S. E., Mishchenko, M. I., Laci, A. A., Zhang, S., Perlwitz, J., and Metzger, S. M.:
694 Do sulfate and nitrate coatings on mineral dust have important effects on radiative
695 properties and climate modeling?, *Journal of Geophysical Research*, 112, D06307
696 doi:10.1029/2005JD006977, 2007.
- 697 Beer, C., Reichstein, M., Tomelleri, E., Ciais, P., Jung, M., Carvalhais, N., Rodenbeck, C.,
698 Arain, M. A., Baldocchi, D., Bonan, G. B., Bondeau, A., Cescatti, A., Lasslop, G.,
699 Lindroth, A., Lomas, M., Luyssaert, S., Margolis, H., Oleson, K. W., Rouspard, O.,
700 Veenendaal, E., Viovy, N., Williams, C., Woodward, F. I., and Papale, D.: Terrestrial
701 Gross Carbon Dioxide Uptake: Global Distribution and Covariation with Climate,
702 *Science*, 329, 834-838, doi:10.1126/Science.1184984, 2010.
- 703 Cirino, G. G., Souza, R. A. F., Adams, D. K., and Artaxo, P.: The effect of atmospheric
704 aerosol particles and clouds on net ecosystem exchange in the Amazon, *Atmospheric
705 Chemistry and Physics*, 14, 6523-6543, doi:10.5194/acp-14-6523-2014, 2014.
- 706 Cohan, D. S., Xu, J., Greenwald, R., Bergin, M. H., and Chameides, W. L.: Impact of
707 atmospheric aerosol light scattering and absorption on terrestrial net primary
708 productivity, *Global Biogeochemical Cycles*, 16, 1090, doi:10.1029/2001gb001441,
709 2002.
- 710 Defries, R. S., Hansen, M. C., Townshend, J. R. G., Janetos, A. C., and Loveland, T. R.: A
711 new global 1-km dataset of percentage tree cover derived from remote sensing, *Global
712 Change Biology*, 6, 247-254, doi:10.1046/J.1365-2486.2000.00296.X, 2000.
- 713 Farquhar, G. D., Caemmerer, S. V., and Berry, J. A.: A Biochemical-Model of
714 Photosynthetic Co₂ Assimilation in Leaves of C-3 Species, *Planta*, 149, 78-90,
715 doi:10.1007/Bf00386231, 1980.
- 716 Felzer, B., Kicklighter, D., Melillo, J., Wang, C., Zhuang, Q., and Prinn, R.: Effects of
717 ozone on net primary production and carbon sequestration in the conterminous United

718 States using a biogeochemistry model, *Tellus Series B-Chemical and Physical*
719 *Meteorology*, 56, 230-248, doi:Doi 10.1111/J.1600-0889.2004.00097.X, 2004.

720 Felzer, B. S., Cronin, T., Reilly, J. M., Melillo, J. M., and Wang, X.: Impacts of ozone on
721 trees and crops, *C. R. Geoscience*, 229, doi:10.1016/j.crte.2007.08.008, 2007.

722 Folini, D., and Wild, M.: The effect of aerosols and sea surface temperature on China's
723 climate in the late twentieth century from ensembles of global climate simulations, *J.*
724 *Geophys. Res.*, 12, 2261-2279, doi:10.1002/2014JD022851, 2015.

725 Gu, L. H., Baldocchi, D. D., Wofsy, S. C., Munger, J. W., Michalsky, J. J., Urbanski, S.
726 P., and Boden, T. A.: Response of a deciduous forest to the Mount Pinatubo eruption:
727 Enhanced photosynthesis, *Science*, 299, 2035-2038, doi:10.1126/science.1078366,
728 2003.

729 Gu, Y., Liou, K. N., Xue, Y., Mechoso, C. R., Li, W., and Luo, Y.: Climatic effects of
730 different aerosol types in China simulated by the UCLA general circulation model,
731 *Journal of Geophysical Research*, 111, D15201, doi:10.1029/2005JD006312, 2006.

732 Hansen, M. C., DeFries, R. S., Townshend, J. R. G., Carroll, M., Dimiceli, C., and
733 Sohlberg, R. A.: Global Percent Tree Cover at a Spatial Resolution of 500 Meters:
734 First Results of the MODIS Vegetation Continuous Fields Algorithm, *Earth*
735 *Interactions*, 7, 1-15, doi:10.1175/1087-3562(2003)007<0001:GPTCAA>2.0.CO;2,
736 2003.

737 Huang, Y., Chameides, W. L., and Dickinson, R. E.: Direct and indirect effects of
738 anthropogenic aerosols on regional precipitation over east Asia, *Journal of*
739 *Geophysical Research*, 112, D03212, doi:10.1029/2006JD007114, 2007.

740 Jing, X., Huang, J., Wang, G., Higuchi, K., Bi, J., Sun, Y., Yu, H., and Wang, T.: The
741 effects of clouds and aerosols on net ecosystem CO₂ exchange over semi-arid Loess
742 Plateau of Northwest China, *Atmospheric Chemistry and Physics*, 10, 8205-8218,
743 doi:10.5194/acp-10-8205-2010, 2010.

744 Jung, M., Reichstein, M., and Bondeau, A.: Towards global empirical upscaling of
745 FLUXNET eddy covariance observations: validation of a model tree ensemble
746 approach using a biosphere model, *Biogeosciences*, 6, 2001-2013, doi:10.5194/bg-6-
747 2001-2009, 2009.

748 Kanniah, K. D., Beringer, J., North, P., and Hutley, L.: Control of atmospheric particles on
749 diffuse radiation and terrestrial plant productivity: A review, *Progress in Physical*
750 *Geography*, 36, 209-237, doi:10.1177/0309133311434244, 2012.

751 Knohl, A., and Baldocchi, D. D.: Effects of diffuse radiation on canopy gas exchange
752 processes in a forest ecosystem, *Journal of Geophysical Research*, 113, G02023,
753 doi:10.1029/2007JG000663, 2008.

754 Liu, Y., Sun, J., and Yang, B.: The effects of black carbon and sulphate aerosols in China
755 regions on East Asia monsoons, *Tellus Series B-Chemical and Physical Meteorology*,
756 61B, 642-656, doi:10.1111/j.1600-0889.2009.00427.x, 2009.

757 Liu, Z., Guan, D. B., Wei, W., Davis, S. J., Ciais, P., Bai, J., Peng, S. S., Zhang, Q.,
758 Hubacek, K., Marland, G., Andres, R. J., Crawford-Brown, D., Lin, J. T., Zhao, H. Y.,
759 Hong, C. P., Boden, T. A., Feng, K. S., Peters, G. P., Xi, F. M., Liu, J. G., Li, Y., Zhao,
760 Y., Zeng, N., and He, K. B.: Reduced carbon emission estimates from fossil fuel
761 combustion and cement production in China, *Nature*, 524, 335-338,
762 doi:10.1038/nature14677, 2015.

- 763 Lombardozi, D., Sparks, J. P., and Bonan, G.: Integrating O₃ influences on terrestrial
764 processes: photosynthetic and stomatal response data available for regional and global
765 modeling, *Biogeosciences*, 10, 6815-6831, doi:10.5194/bg-10-6815-2013, 2013.
- 766 Menon, S., and Rotstayn, L.: The radiative influence of aerosol effects on liquid-phase
767 cumulus and stratiform clouds based on sensitivity studies with two climate models,
768 *Climate Dynamics*, 27, 345-356, doi:10.1007/s00382-006-0139-3, 2006.
- 769 Mercado, L. M., Bellouin, N., Sitch, S., Boucher, O., Huntingford, C., Wild, M., and Cox,
770 P. M.: Impact of changes in diffuse radiation on the global land carbon sink, *Nature*,
771 458, 1014-1017, doi:Doi 10.1038/Nature07949, 2009.
- 772 Oleson, K. W., Lawrence, D. M., Bonan, G. B., Flanne, M. G., Kluzek, E., Lawrence, P.
773 J., Levis, S., Swenson, S. C., and Thornton, P. E.: Technical Description of version 4.0
774 of the Community Land Model (CLM), National Center for Atmospheric Research,
775 Boulder, CONCAR/TN-478+STR, 2010.
- 776 Ollinger, S. V., Aber, J. D., Reich, P. B., and Freuder, R. J.: Interactive effects of nitrogen
777 deposition, tropospheric ozone, elevated CO₂ and land use history on the carbon
778 dynamics of northern hardwood forests, *Global Change Biology*, 8, 545-562,
779 doi:10.1046/J.1365-2486.2002.00482.X, 2002.
- 780 Piao, S. L., Fang, J. Y., Ciais, P., Peylin, P., Huang, Y., Sitch, S., and Wang, T.: The carbon
781 balance of terrestrial ecosystems in China, *Nature*, 458, 1009-1013,
782 doi:10.1038/nature07944, 2009.
- 783 Piao, S. L., Sitch, S., Ciais, P., Friedlingstein, P., Peylin, P., Wang, X. H., Ahlstrom, A.,
784 Anav, A., Canadell, J. G., Cong, N., Huntingford, C., Jung, M., Levis, S., Levy, P. E.,
785 Li, J. S., Lin, X., Lomas, M. R., Lu, M., Luo, Y. Q., Ma, Y. C., Myneni, R. B., Poulter,
786 B., Sun, Z. Z., Wang, T., Viovy, N., Zaehle, S., and Zeng, N.: Evaluation of terrestrial
787 carbon cycle models for their response to climate variability and to CO₂ trends, *Global
788 Change Biology*, 19, 2117-2132, doi:10.1111/Gcb.12187, 2013.
- 789 Pickering, K. E., Wang, Y., Tao, W.-K., Price, C., and Müller, J.-F.: Vertical distributions
790 of lightning NO_x for use in regional and global chemical transport models, *Journal of
791 Geophysical Research*, 103, 31203-31216, doi:10.1029/98JD02651, 1998.
- 792 Price, C., Penner, J., and Prather, M.: NO_x from lightning: 1. Global distribution based on
793 lightning physics, *Journal of Geophysical Research*, 102, 5929-5941,
794 doi:10.1029/96JD03504, 1997.
- 795 Qian, Y., Leung, L. R., Ghan, S. J., and Giorgi, F.: Regional climate effects of aerosols
796 over China: modeling and observation, *Tellus Series B-Chemical and Physical
797 Meteorology*, 55, 914-934, doi:10.1046/j.1435-6935.2003.00070.x, 2003.
- 798 Reich, P. B., and Amundson, R. G.: Ambient Levels of Ozone Reduce Net Photosynthesis
799 in Tree and Crop Species, *Science*, 230, 566-570, doi:10.1126/science.230.4725.566,
800 1985.
- 801 Ren, W., Tian, H., Tao, B., Chappelka, A., Sun, G., Lu, C., Liu, M., Chen, G., and Xu, X.:
802 Impacts of tropospheric ozone and climate change on net primary productivity and net
803 carbon exchange of China's forest ecosystems, *Global Ecology & Biogeography*, 20,
804 391-406, doi:10.1111/j.1466-8238.2010.00606.x, 2011.
- 805 Rienecker, M. M., Suarez, M. J., Gelaro, R., Todling, R., Bacmeister, J., Liu, E.,
806 Bosilovich, M. G., Schubert, S. D., Takacs, L., Kim, G. K., Bloom, S., Chen, J. Y.,
807 Collins, D., Conaty, A., Da Silva, A., Gu, W., Joiner, J., Koster, R. D., Lucchesi, R.,
808 Molod, A., Owens, T., Pawson, S., Pegion, P., Redder, C. R., Reichle, R., Robertson,

809 F. R., Ruddick, A. G., Sienkiewicz, M., and Woollen, J.: MERRA: NASA's Modern-
810 Era Retrospective Analysis for Research and Applications, *Journal of Climate*, 24,
811 3624-3648, doi:10.1175/Jcli-D-11-00015.1, 2011.

§12 Rocha, A. V., Su, H. B., Vogel, C. S., Schmid, H. P., and Curtis, P. S.: Photosynthetic and
813 water use efficiency responses to diffuse radiation by an aspen-dominated northern
814 hardwood forest, *Forest Science*, 50, 793-801, 2004.

§15 Schaefer, K., Schwalm, C. R., Williams, C., Arain, M. A., Barr, A., Chen, J. M., Davis, K.
816 J., Dimitrov, D., Hilton, T. W., Hollinger, D. Y., Humphreys, E., Poulter, B., Raczka,
817 B. M., Richardson, A. D., Sahoo, A., Thornton, P., Vargas, R., Verbeeck, H.,
818 Anderson, R., Baker, I., Black, T. A., Bolstad, P., Chen, J. Q., Curtis, P. S., Desai, A.
819 R., Dietze, M., Dragoni, D., Gough, C., Grant, R. F., Gu, L. H., Jain, A., Kucharik, C.,
820 Law, B., Liu, S. G., Lokipitiya, E., Margolis, H. A., Matamala, R., McCaughey, J. H.,
821 Monson, R., Munger, J. W., Oechel, W., Peng, C. H., Price, D. T., Ricciuto, D., Riley,
822 W. J., Roulet, N., Tian, H. Q., Tonitto, C., Torn, M., Weng, E. S., and Zhou, X. L.: A
823 model-data comparison of gross primary productivity: Results from the North
824 American Carbon Program site synthesis, *J. Geophys. Res.*, 117, G03010,
825 doi:10.1029/2012jg001960, 2012.

§26 Schmidt, G. A., [Ruedy, R.](#), [Hansen, J. E.](#), [Aleinov, I.](#), [Bell, N.](#), [Bauer, M.](#), [Bauer, S.](#), [Cairns,](#)
827 [B.](#), [Canuto, V.](#), [Cheng, Y.](#), [Del Genio, A.](#), [Faluvegi, G.](#), [Friend, A. D.](#), [Hall, T. M.](#), [Hu,](#)
828 [Y. Y.](#), [Kelley, M.](#), [Kiang, N. Y.](#), [Koch, D.](#), [Lacis, A. A.](#), [Lerner, J.](#), [Lo, K. K.](#), [Miller,](#)
829 [R. L.](#), [Nazarenko, L.](#), [Oinas, V.](#), [Perlwitz, J.](#), [Perlwitz, J.](#), [Rind, D.](#), [Romanou, A.](#),
830 [Russell, G. L.](#), [Sato, M.](#), [Shindell, D. T.](#), [Stone, P. H.](#), [Sun, S.](#), [Tausnev, N.](#), [Thresher,](#)
831 [D.](#), and [Yao, M. S.](#): Present-day atmospheric simulations using GISS ModelE:
832 [Comparison to in situ, satellite, and reanalysis data](#), *Journal of Climate*, 19, 153-192,
833 doi:10.1175/Jcli3612.1, 2006.

§34 [Schmidt, G. A.](#), Kelley, M., Nazarenko, L., Ruedy, R., Russell, G. L., Aleinov, I., Bauer,
835 M., Bauer, S. E., Bhat, M. K., Bleck, R., Canuto, V., Chen, Y. H., Cheng, Y., Clune,
836 T. L., Del Genio, A., de Fainchtein, R., Faluvegi, G., Hansen, J. E., Healy, R. J., Kiang,
837 N. Y., Koch, D., Lacis, A. A., LeGrande, A. N., Lerner, J., Lo, K. K., Matthews, E. E.,
838 Menon, S., Miller, R. L., Oinas, V., Olosio, A. O., Perlwitz, J. P., Puma, M. J., Putman,
839 W. M., Rind, D., Romanou, A., Sato, M., Shindell, D. T., Sun, S., Syed, R. A.,
840 Tausnev, N., Tsigaridis, K., Unger, N., Voulgarakis, A., Yao, M. S., and Zhang, J. L.:
841 Configuration and assessment of the GISS ModelE2 contributions to the CMIP5
842 archive, *Journal of Advances in Modeling Earth Systems*, 6, 141-184,
843 doi:10.1002/2013ms000265, 2014.

§44 Shao, J., Zhou, X. H., Luo, Y. Q., Zhang, G. D., Yan, W., Li, J. X., Li, B., Dan, L., Fisher,
845 J. B., Gao, Z. Q., He, Y., Huntzinger, D., Jain, A. K., Mao, J. F., Meng, J. H., Michalak,
846 A. M., Parazoo, N. C., Peng, C. H., Poulter, B., Schwalm, C. R., Shi, X. Y., Sun, R.,
847 Tao, F. L., Tian, H. Q., Wei, Y. X., Zeng, N., Zhu, Q., and Zhu, W. Q.: Uncertainty
848 analysis of terrestrial net primary productivity and net biome productivity in China
849 during 1901-2005, *Journal of Geophysical Research*, 121, 1372-1393,
850 doi:10.1002/2015jg003062, 2016.

§51 Shindell, D. T., Pechony, O., Voulgarakis, A., Faluvegi, G., Nazarenko, L., Lamarque, J.
852 F., Bowman, K., Milly, G., Kovari, B., Ruedy, R., and Schmidt, G. A.: Interactive
853 ozone and methane chemistry in GISS-E2 historical and future climate simulations,

Formatted: Justified

854 Atmospheric Chemistry and Physics, 13, 2653-2689, doi:10.5194/Acp-13-2653-2013,
855 2013.

856 Sitch, S., Cox, P. M., Collins, W. J., and Huntingford, C.: Indirect radiative forcing of
857 climate change through ozone effects on the land-carbon sink, *Nature*, 448, 791-794,
858 doi:10.1038/Nature06059, 2007.

859 Spitters, C. J. T.: Separating the Diffuse and Direct Component of Global Radiation and
860 Its Implications for Modeling Canopy Photosynthesis .2. Calculation of Canopy
861 Photosynthesis, *Agricultural and Forest Meteorology*, 38, 231-242, doi:10.1016/0168-
862 1923(86)90061-4, 1986.

863 Spracklen, D. V., Arnold, S. R., and Taylor, C. M.: Observations of increased tropical
864 rainfall preceded by air passage over forests, *Nature*, 489, 282-285,
865 doi:10.1038/nature11390, 2012.

866 Steiner, A. L., and Chameides, W. L.: Aerosol-induced thermal effects increase modelled
867 terrestrial photosynthesis and transpiration, *Tellus Series B-Chemical and Physical
868 Meteorology*, 57, 404-411, doi:DOI 10.1111/j.1600-0889.2005.00158.x, 2005.

869 Strada, S., Unger, N., and Yue, X.: Observed aerosol-induced radiative effect on plant
870 productivity in the eastern United States, *Atmospheric Environment*, 122, 463-476,
871 doi:10.1016/j.atmosenv.2015.09.051, 2015.

872 Tian, H. Q., Melillo, J., Lu, C. Q., Kicklighter, D., Liu, M. L., Ren, W., Xu, X. F., Chen,
873 G. S., Zhang, C., Pan, S. F., Liu, J. Y., and Running, S.: China's terrestrial carbon
874 balance: Contributions from multiple global change factors, *Global Biogeochemical
875 Cycles*, 25, Gb1007, doi:10.1029/2010gb003838, 2011.

876 Unger, N., Harper, K., Zheng, Y., Kiang, N. Y., Aleinov, I., Arneth, A., Schurgers, G.,
877 Amelynck, C., Goldstein, A., Guenther, A., Heinesch, B., Hewitt, C. N., Karl, T.,
878 Laffineur, Q., Langford, B., McKinney, K. A., Misztal, P., Potosnak, M., Rinne, J.,
879 Pressley, S., Schoon, N., and Serça, D.: Photosynthesis-dependent isoprene emission
880 from leaf to planet in a global carbon-chemistry-climate model, *Atmos. Chem. Phys.*,
881 13, 17717-17791, doi:10.5194/acp-13-10243-2013, 2013.

882 Unger, N., and Yue, X.: Strong chemistry-climate feedbacks in the Pliocene, *Geophysical
883 Research Letters*, 41, 527-533, doi:10.1002/2013gl058773, 2014.

884 van Vuuren, D. P., Edmonds, J., Kainuma, M., Riahi, K., Thomson, A., Hibbard, K., Hurtt,
885 G. C., Kram, T., Krey, V., Lamarque, J. F., Masui, T., Meinshausen, M., Nakicenovic,
886 N., Smith, S. J., and Rose, S. K.: The representative concentration pathways: an
887 overview, *Climatic Change*, 109, 5-31, doi:10.1007/s10584-011-0148-z, 2011.

888 Wild, M., Folini, D., Schar, C., Loeb, N., Dutton, E. G., and Konig-Langlo, G.: The global
889 energy balance from a surface perspective, *Climate Dynamics*, 40, 3107-3134,
890 doi:10.1007/s00382-012-1569-8, 2013.

891 Wittig, V. E., Ainsworth, E. A., and Long, S. P.: To what extent do current and projected
892 increases in surface ozone affect photosynthesis and stomatal conductance of trees? A
893 meta-analytic review of the last 3 decades of experiments, *Plant Cell and Environment*,
894 30, 1150-1162, doi:10.1111/J.1365-3040.2007.01717.X, 2007.

895 Xia, X.: A closer looking at dimming and brightening in China during 1961-2005, *Annales
896 Geophysicae*, 28, 1121-1132, doi:10.5194/angeo-28-1121-2010, 2010.

897 Xiao, J. F., Zhou, Y., and Zhang, L.: Contributions of natural and human factors to
898 increases in vegetation productivity in China, *Ecosphere*, 6, 233, doi:10.1890/Es14-
899 00394.1, 2015.

900 Yienger, J. J., and Levy, H.: Empirical-Model of Global Soil-Biogenic Nox Emissions, J.
901 Geophys. Res., 100, 11447-11464, doi:10.1029/95jd00370, 1995.
902 Yue, X., and Unger, N.: Ozone vegetation damage effects on gross primary productivity in
903 the United States, Atmospheric Chemistry and Physics, 14, 9137-9153,
904 doi:10.5194/acp-14-9137-2014, 2014.
905 Yue, X., and Unger, N.: The Yale Interactive terrestrial Biosphere model version 1.0:
906 description, evaluation and implementation into NASA GISS ModelE2, Geoscientific
907 Model Development, 8, 2399-2417, doi:10.5194/gmd-8-2399-2015, 2015.
908 Yue, X., Unger, N., and Zheng, Y.: Distinguishing the drivers of trends in land carbon
909 fluxes and biogenic emissions over the past three decades, Atmospheric Chemistry and
910 Physics, 15, 11931-11948, doi:10.5194/acp-15-11931-2015, 2015.
911 Yue, X., Keenan, T. F., Munger, W., and Unger, N.: Limited effect of ozone reductions on
912 the 20-year photosynthesis trend at Harvard forest, Global Change Biology, 22, 3750-
913 3759, doi:10.1111/gcb.13300, 2016.
914 Yue, X., and Unger, N.: Aerosol optical depth thresholds as a tool to assess diffuse radiation
915 fertilization of the land carbon uptake in China, Atmospheric Chemistry and Physics,
916 17, 1329-1342, doi:10.5194/acp-17-1329-2017, 2017.
917 Zhao, M. S., Heinsch, F. A., Nemani, R. R., and Running, S. W.: Improvements of the
918 MODIS terrestrial gross and net primary production global data set, Remote Sensing
919 of Environment, 95, 164-176, doi:10.1016/J.Rse.2004.12.011, 2005.
920 Zhou, Y., Xing, X., Lang, J., Chen, D., Cheng, S., Wei, L., Wei, X., and Liu, C.: A
921 comprehensive biomass burning emission inventory with high spatial and temporal
922 resolution in China, Atmospheric Chemistry and Physics, 17, 2839-2864,
923 doi:10.5194/acp-17-2839-2017, 2017.
924
925

Formatted: Justified

926
927
928
929

Table 1. Summary of models and simulations

Model Name	Model class	Climate drivers	Number of runs	Table index ^a	Purpose
ModelE2-YIBs	Coupled climate model	Online	24	2	Calculate Δ NPP by O ₃ and aerosols at 2010 and 2030
YIBs	Vegetation model	MERRA	15	S2	Evaluate O ₃ damage scheme for China PFTs
YIBs	Vegetation model	ModelE2-YIBs	30	S3	Isolate aerosol individual climatic impacts on NPP

930
931
932
933

^a Table index refers to the tables in the main text and supporting information.

934
935
936

Table 2. Summary of 24 online simulations with the ModelE2-YIBs model

Simulations	Period	Emission Inventories	Emission sources	Ozone damage	Aerosol indirect effect
G10NATNO3	2010	GAINS ^a	Natural	Null	No
G10ALLNO3	2010	GAINS	All ^d	Null	No
G10ALLLO3	2010	GAINS	All	Low	No
G10ALLHO3	2010	GAINS	All	High	No
G30NATNO3	2030	GAINS CLE ^b	Natural	Null	No
G30ALLNO3	2030	GAINS CLE	All	Null	No
G30ALLLO3	2030	GAINS CLE	All	Low	No
G30ALLHO3	2030	GAINS CLE	All	High	No
M30NATNO3	2030	GAINS MTFR ^c	Natural	Null	No
M30ALLNO3	2030	GAINS MTFR	All	Null	No
M30ALLLO3	2030	GAINS MTFR	All	Low	No
M30ALLHO3	2030	GAINS MTFR	All	High	No
G10NATNO3_AIE	2010	GAINS	Natural	Null	Yes
G10ALLNO3_AIE	2010	GAINS	All	Null	Yes
G10ALLLO3_AIE	2010	GAINS	All	Low	Yes
G10ALLHO3_AIE	2010	GAINS	All	High	Yes
G30NATNO3_AIE	2030	GAINS CLE	Natural	Null	Yes
G30ALLNO3_AIE	2030	GAINS CLE	All	Null	Yes
G30ALLLO3_AIE	2030	GAINS CLE	All	Low	Yes
G30ALLHO3_AIE	2030	GAINS CLE	All	High	Yes
M30NATNO3_AIE	2030	GAINS MTFR	Natural	Null	Yes
M30ALLNO3_AIE	2030	GAINS MTFR	All	Null	Yes
M30ALLLO3_AIE	2030	GAINS MTFR	All	Low	Yes
M30ALLHO3_AIE	2030	GAINS MTFR	All	High	Yes

937 ^a GAINS is short for the v4a emission inventory of Greenhouse Gas and Air Pollution
938 Interactions and Synergies (<http://gains.iiasa.ac.at/models/index.html>).

939 ^b CLE is the emission scenario predicted based on current legislation emissions.

940 ^c MTFR is the emission scenario predicted with maximum technically feasible reductions.

941 ^d All emissions including both natural and anthropogenic sources. For the detailed
942 anthropogenic emissions, refer to Fig. S2.

943

944
 945
 946
 947
 948

Table 3. Changes in NPP over China due to combined and separate effects^a of air pollution (units: Pg C yr⁻¹)

	2010	2030 CLE	2030 MTR
O₃ (mean)^b	-0.59 ± 0.11 (-0.60 ± 0.13)	-0.67 ± 0.11 (-0.71 ± 0.16)	-0.29 ± 0.14 (-0.31 ± 0.10)
Low sensitivity	-0.43 ± 0.12 (-0.40 ± 0.13)	-0.43 ± 0.14 (-0.51 ± 0.16)	-0.22 ± 0.17 (-0.15 ± 0.10)
High sensitivity	-0.76 ± 0.15 (-0.80 ± 0.16)	-0.90 ± 0.13 (-0.92 ± 0.18)	-0.36 ± 0.16 (-0.46 ± 0.12)
Aerosol (total)^c	0.20 ± 0.08 (-0.20 ± 0.09)	0.23 ± 0.14 (-0.09 ± 0.19)	0.16 ± 0.14 (0.04 ± 0.17)
Temperature ^d	0.03 ± 0.04 (0.01 ± 0.04)	0.04 ± 0.02 (0.02 ± 0.05)	0.03 ± 0.04 (0.00 ± 0.04)
Radiation ^d	0.09 ± 0.04 (-0.03 ± 0.04)	0.16 ± 0.06 (-0.01 ± 0.06)	0.11 ± 0.04 (-0.03 ± 0.03)
Soil moisture ^d	0.07 ± 0.07 (-0.19 ± 0.10)	0.01 ± 0.09 (-0.09 ± 0.15)	0.03 ± 0.12 (0.00 ± 0.09)
O₃ + aerosol (net)^e	-0.39 ± 0.12 (-0.80 ± 0.11)	-0.43 ± 0.12 (-0.80 ± 0.10)	-0.12 ± 0.13 (-0.28 ± 0.14)

949
 950 ^a Results shown are the averages ± one standard deviation. Simulations with both aerosol
 951 direct and indirect radiative effects (AIE) are shown in the brackets.

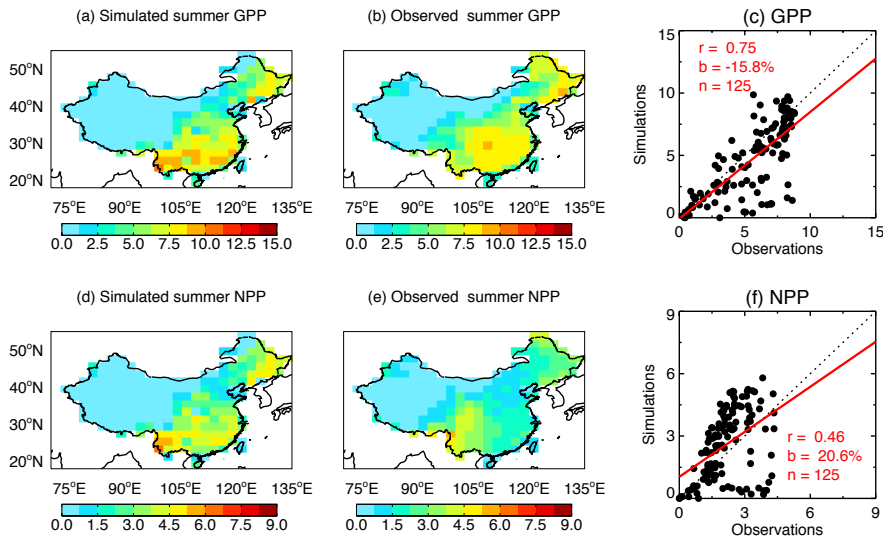
952 ^b Mean O₃ damages are calculated as half of differences in ΔNPP between low and high
 953 sensitivities, e.g., present-day mean O₃ damage is $\frac{1}{2}(G10ALLHO3+G10ALLLO3) -$
 954 G10ALLNO3.

955 ^c Combined aerosol effects are calculated with the ModelE2-YIBs climate model, e.g.,
 956 present-day aerosol effect is G10ALLNO3 – G10NATNO3.

957 ^d Separate aerosol effects are calculated with the offline YIBs vegetation model driven with
 958 forcings from the climate model (Table S3).

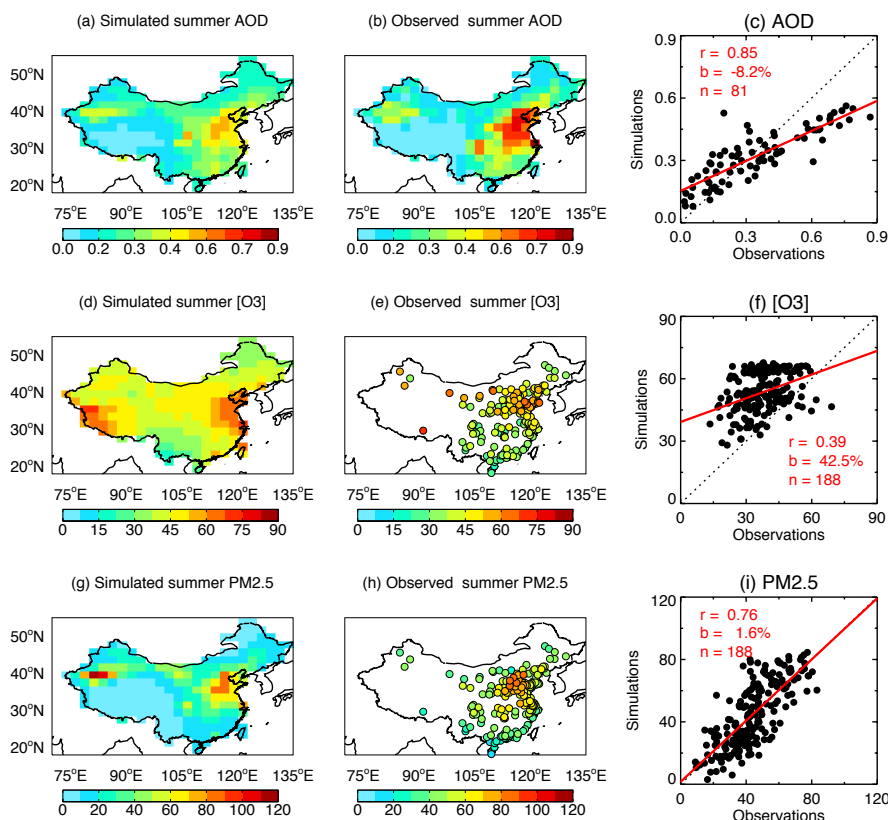
959 ^e The net impact of O₃ damages and aerosol effects, for example at present day, is
 960 calculated as $\frac{1}{2}(G10ALLHO3+G10ALLLO3) - G10NATNO3$.

961
 962
 963
 964
 965
 966
 967



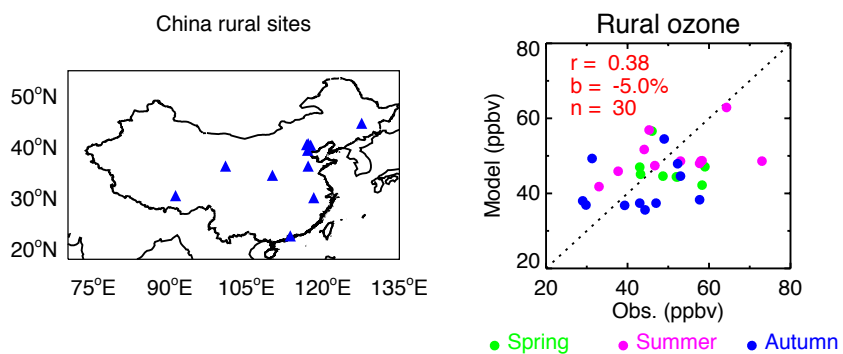
968
 969
 970
 971
 972
 973
 974
 975
 976
 977
 978

Figure 1. Evaluation of simulated summertime carbon fluxes by ModelE2-YIBs. Panels show GPP (top row) and NPP (bottom row) over China. Simulation results (a, d) are the average of G10ALLHO3 and G10ALLLO3, which are performed with the climate model ModelE2-YIBs using high and low ozone damage sensitivities (Table 2). The correlation coefficients (r), relative biases (b), and number of grid cells (n) for the comparisons are listed on the scatter plots. Units: $\text{g C m}^{-2} \text{ day}^{-1}$.



981
982
983 **Figure 2.** Evaluation of simulated summertime air pollution in China. Evaluations shown
984 include (a) aerosol optical depth (AOD) at 550 nm, (d) $[O_3]$ (units: ppbv), and (g) $PM_{2.5}$
985 concentrations (units: $\mu g\ m^{-3}$) with observations from (b) the satellite retrieval of the
986 MODIS (averaged for 2008-2012), and (e) and (h) measurements from 188 ground-based
987 sites (at the year 2014). Simulation results are from G10ALLNO3 performed with the
988 climate model ModelE2-YIBs (Table 2). The correlation coefficients (r), relative biases
989 (b), and number of sites/grids (n) for the comparisons are listed on the scatter plots.

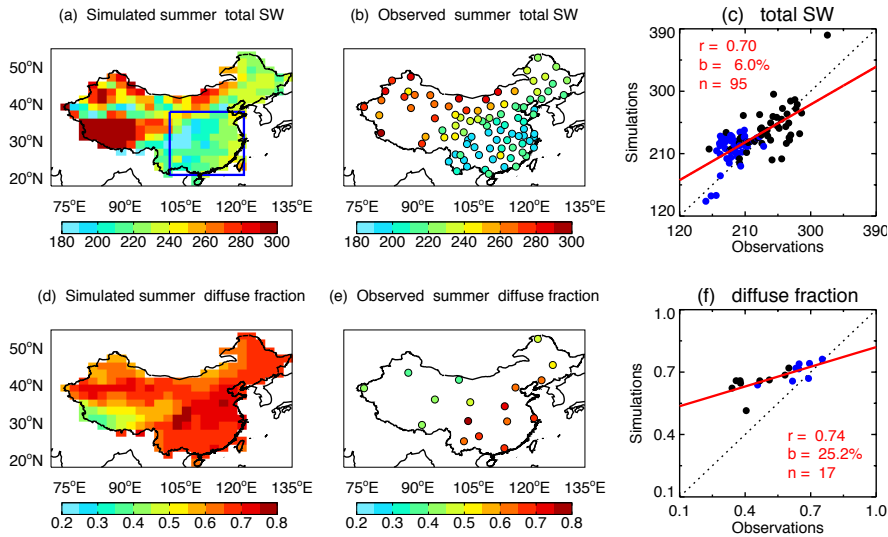
992
993



994
995 **Figure 3.** Evaluation of simulated [O₃] at rural sites in China. Simulation results are from
996 G10ALLNO3 performed with the climate model ModelE2-YIBs (Table 2). For the scatter
997 plots, green, pink, and blue points represent values in spring, summer, and autumn,
998 respectively. The data sources of all sites are listed in Table S4.

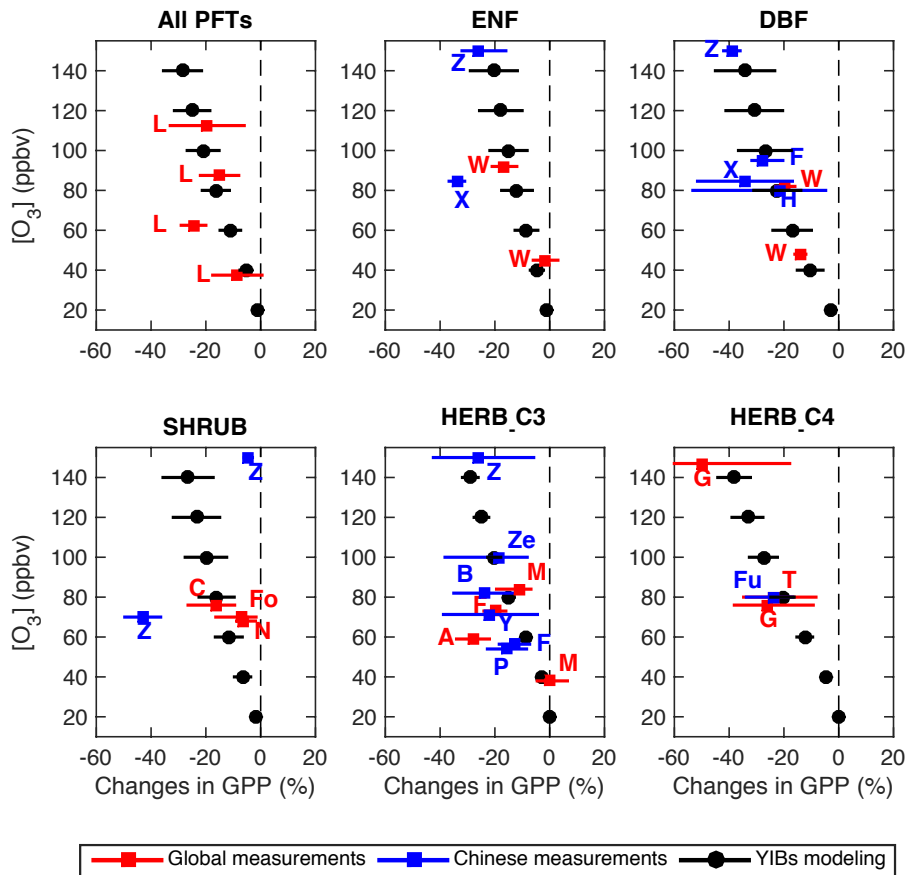
999
1000

1001
1002
1003



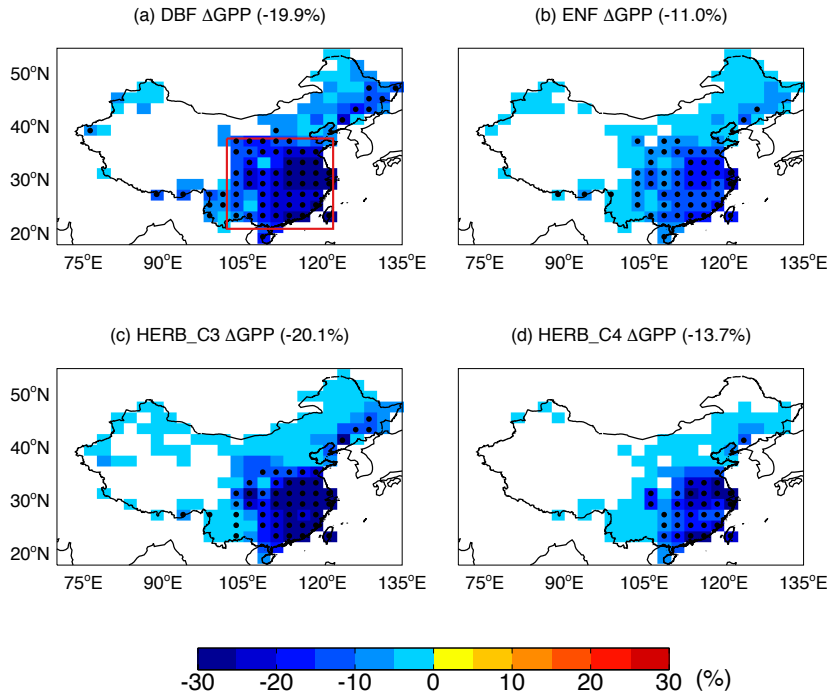
1004
1005
1006
1007
1008
1009
1010
1011
1012
1013

Figure 4. Evaluation of simulated radiation fluxes by ModelE2-YIBs. Panels show summertime surface (a) total shortwave radiation (units: $W m^{-2}$) and (d) diffuse-to-total fraction with (b, e) observations from 106 sites. Simulation results are from G10ALLNO3 performed with the climate model ModelE2-YIBs (Table 2). The correlation coefficients (r), relative biases (b), and number of sites (n) for the comparisons are listed on the (c, f) scatter plots. The blue points in the scatter plots represent sites located within the box regions in southeastern China as shown in (a).



1014
 1015 **Figure 5.** Comparison of predicted changes in summer GPP by O_3 with measurements.
 1016 Simulations are performed using the offline YIBs vegetation model (Table S2) and
 1017 averaged for all grid squares over China weighted by the area of a specific PFT. Black
 1018 points show the simulated mean reductions with error bars indicating damage range from
 1019 low to high O_3 sensitivity. Solid squares with error bars show the results (mean plus
 1020 uncertainty) based on measurements reported in the literature (Table S1). Experiments
 1021 performed for vegetation types in China are denoted with blue symbols. The author initials
 1022 are indicated for the corresponding studies.

1023
1024



1025
1026
1027

Figure 6. Predicted offline percentage damage to summer GPP caused by O₃. Panels show the damages to (a) ENF (evergreen needleleaf forest), (b) DBF (deciduous broadleaf forest), (c) C3 herbs, and (d) C4 herbs over China in the year 2010. Simulations are performed with the climate model ModelE2-YIBs, which does not feed O₃ vegetation damages back to affect biometeorology, plant growth, and ecosystem physiology. The results are averaged for the low and high damaging sensitivities:

1033

$$\left(\frac{1}{2}(G10ALLHO3_OFF+G10ALLLO3_OFF)/G10ALLNO3 - 1\right) \times 100\%$$

1034

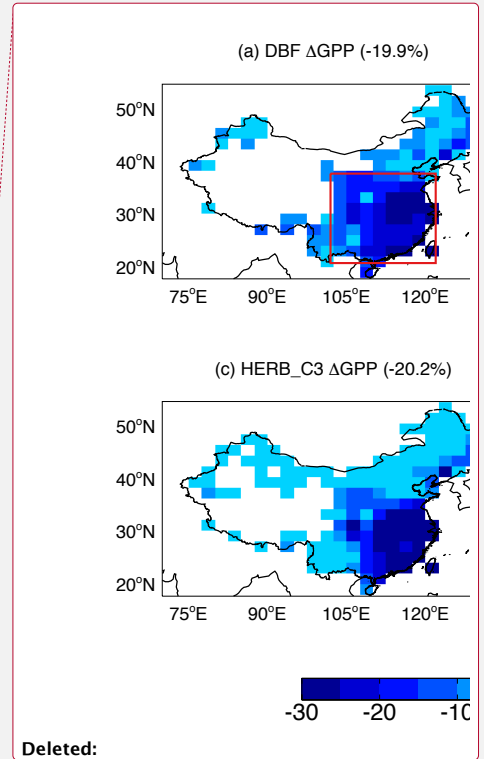
The average value over the box domain of (a) is shown in the title bracket of each subpanel.

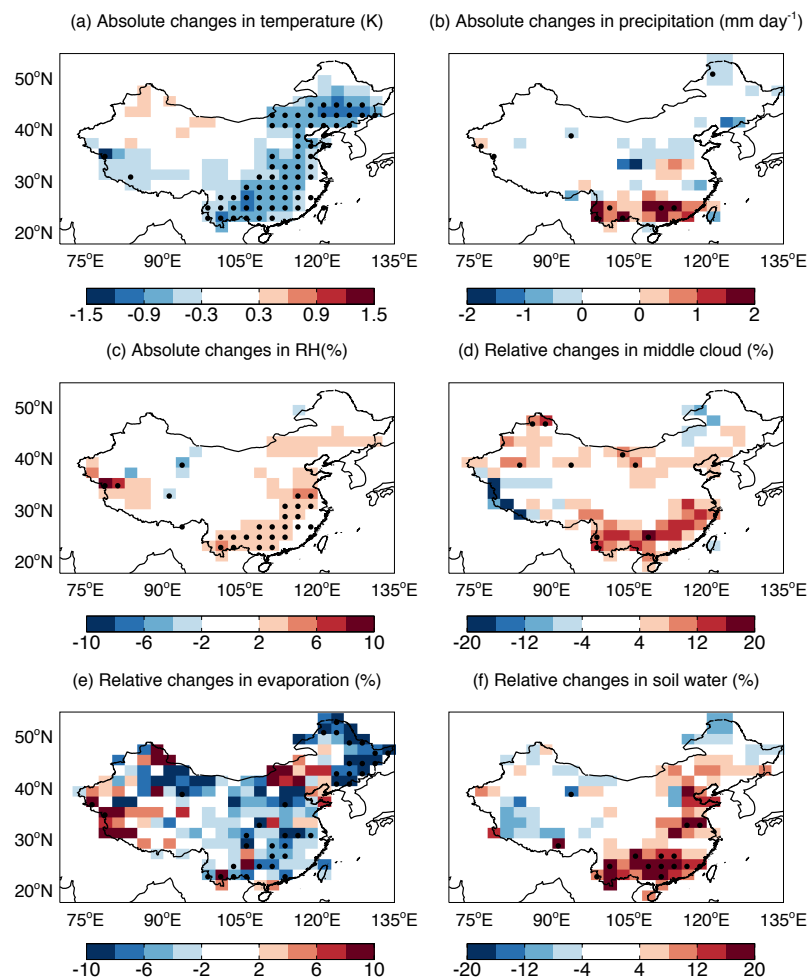
1035

Significant changes ($p < 0.05$) are marked with black dots.

1036

1037

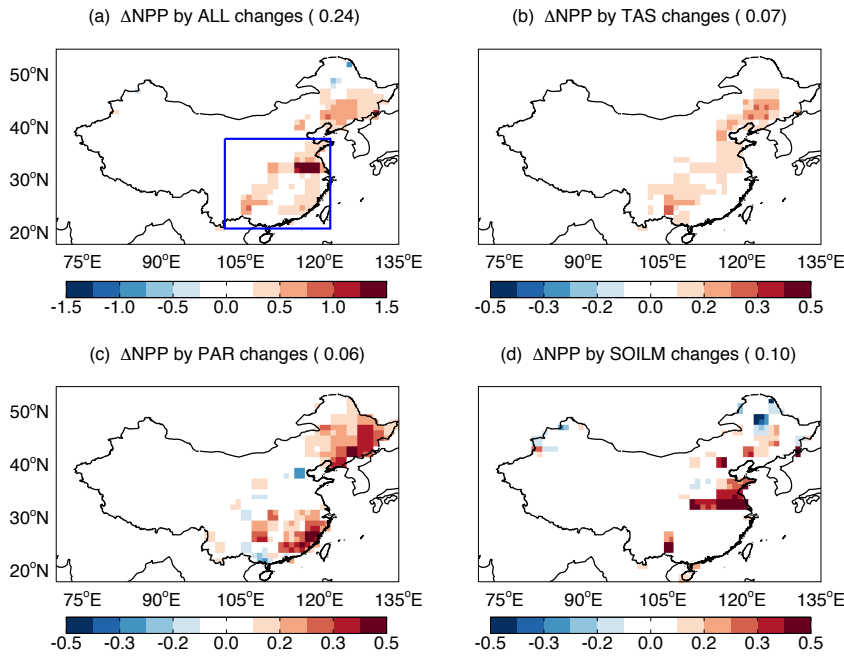




1039
 1040
 1041
 1042
 1043
 1044
 1045
 1046
 1047
 1048

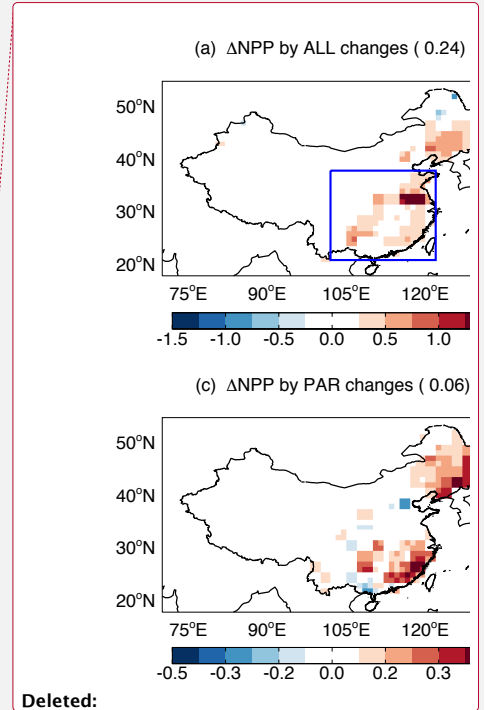
Figure 7. Changes in summer meteorology due to direct radiative effects of anthropogenic aerosols. All changes are calculated as the differences between the simulations G10ALLNO3 and G10NATNO3. For (a) temperature, (b) precipitation, and (c) relative humidity, we show the absolute changes as $G10ALLNO3 - G10NATNO3$. For (d) middle cloud cover, (e) evaporation, and (f) soil water content, we show the relative changes as $(G10ALLNO3/G10NATNO3 - 1) \times 100\%$. Significant changes ($p < 0.05$) are marked with black dots.

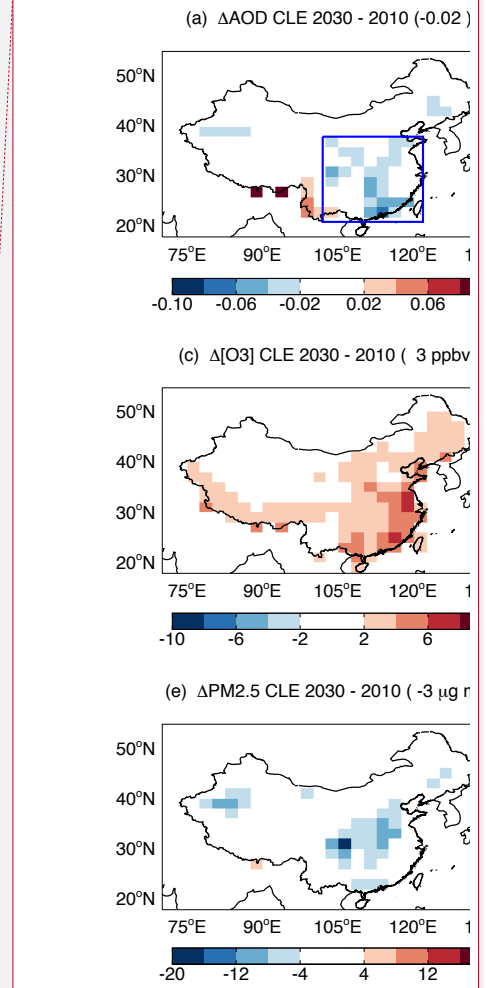
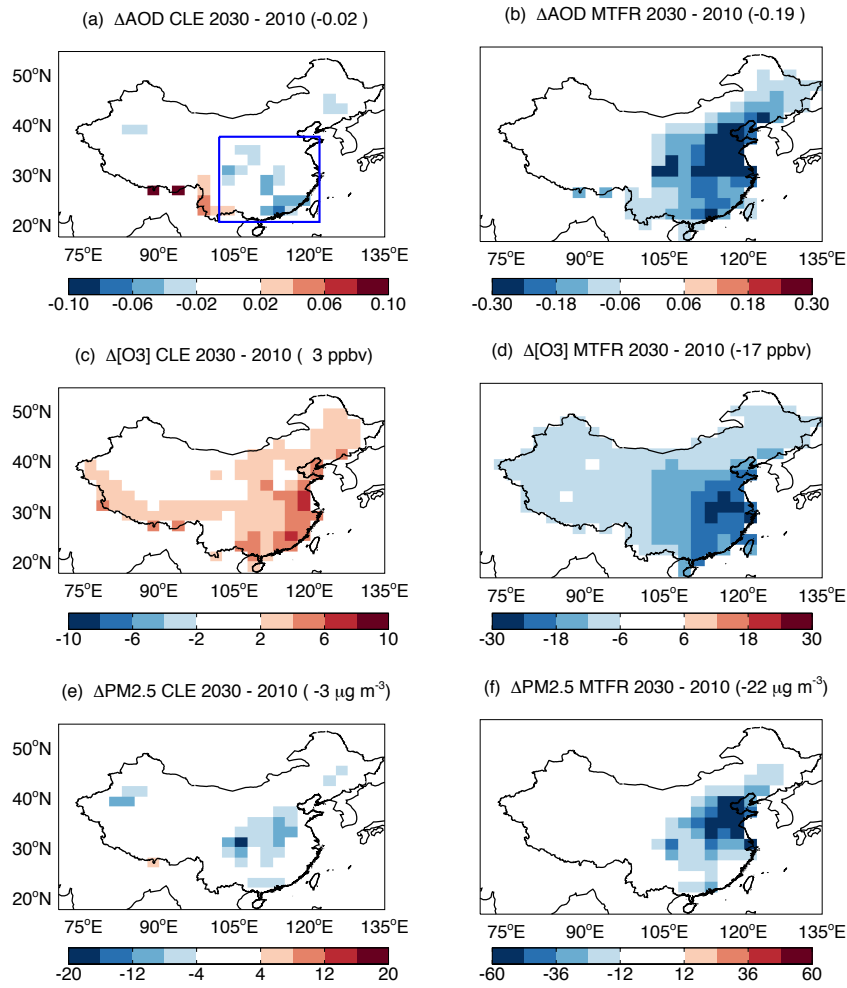
1049
1050
1051



1052
1053
1054
1055
1056
1057
1058
1059
1060
1061
1062
1063
1064

Figure 8. Decomposition of aerosol-induced changes in summer NPP. Changes in NPP are caused by aerosol-induced changes in (b) surface air temperature, (c) photosynthetically active radiation (PAR), (d) soil moisture, and (a) the combination of above three effects. Simulations are performed with the offline YIBs vegetation model driven with meteorological forcings simulated with the ModelE2-YIBs climate model (Table S3). The NPP responses to PAR include the DRF effects. The color scale for the first panel is different from the others. The average NPP perturbation over the box domain in a is shown in the bracket of each title. Only the significant changes ($p < 0.05$) are shown. Units: $\text{g C m}^{-2} \text{ day}^{-1}$.

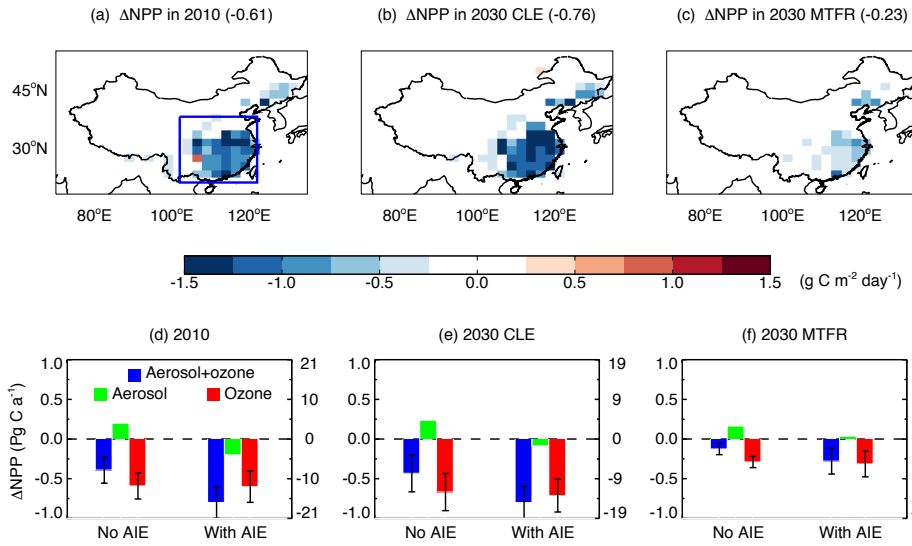




Deleted:

1066
 1067 **Figure 9.** Predicted changes in summertime air pollution by 2030. Panels shown are for (a,
 1068 b) AOD, (c, d) $[\text{O}_3]$, and (e, f) $\text{PM}_{2.5}$ concentrations for the year 2030 relative to 2010 based
 1069 on scenarios of (left) current legislation emissions (CLE) and (right) maximum technically
 1070 feasible reduction (MTFR). Results for the left panels are calculated as (G30ALLNO3 –
 1071 G10ALLNO3). Results for the right panels are calculated as (M30ALLNO3 –
 1072 G10ALLNO3). The average value over the box domain of (a) is shown in the title bracket
 1073 of each subpanel. Only the significant changes ($p < 0.05$) are shown.

1075
1076



1077
1078

1079 **Figure 10.** Impacts of air pollution on NPP in the whole of China. Results shown are
1080 combined effects of aerosol and O_3 on the summer NPP in (a) 2010, (b) 2030 with CLE
1081 scenario, and (c) 2030 with MTRF scenario. Results for the top panels do not include
1082 aerosol indirect effects (AIE) but do include the meteorological response to aerosol direct
1083 radiative effects. The average NPP perturbation over the box domain in (a) is shown in the
1084 bracket of each title. The perturbations to annual total NPP by aerosol, O_3 , and their sum
1085 over the whole China are shown in (d-f) for different periods, with (right) and without (left)
1086 inclusion of AIE. Damages by O_3 are averaged for low and high sensitivities with error
1087 bars indicating ranges. The percentage changes are calculated based on NPP without AIE.
1088 Simulations are performed with the ModelE2-YIBs model. Only the significant changes (p
1089 < 0.05) are shown in (a-c).

1090
1091